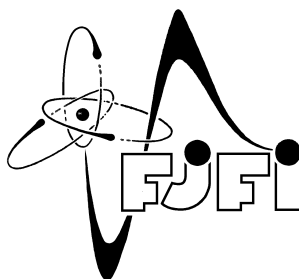


CZECH TECHNICAL UNIVERSITY IN PRAGUE  
FACULTY OF NUCLEAR SCIENCES AND PHYSICAL ENGINEERING



# BACHELOR THESIS

## ATLAS INNER DETECTOR AND ITS TESTING WITH COSMIC MUONS

Tomáš Jakoubek

Supervisor: Prom. fyz. Václav Vrba, CSc.

September 6, 2009



## Acknowledgements

I would like to thank my supervisor Václav Vrba for his invaluable help during creation of this work and for introducing me to CERN and the ATLAS experiment. My big thanks belongs to Attilio Andreazza from the ATLAS Pixel Group, for his help with cosmic muons studies in SR1, and also to my colleagues at the Academy of Sciences of the Czech Republic, especially to Michal Marčišovský and Pavel Jež. And last but not least, I would like to thank my family and friends, especially to Tereza Liepoldová, for their support up until now.

## Prohlášení

Prohlašuji, že jsem svou bakalářskou práci vypracoval samostatně a použil jsem pouze podklady uvedené v příloženém seznamu.

Nemám závažný důvod proti užití tohoto školního díla ve smyslu §60 Zákona č. 121/2000 Sb., o právu autorském, o právech souvisejících s právem autorským a o změně některých zákonů (autorský zákon).

## Declaration

I declare that I wrote my bachelor thesis independently and exclusively with the use of cited bibliography.

I agree with the usage of this thesis in the purport of the Act 121/2000 (Copyright Act).

Prague, September 6, 2009

Tomáš Jakoubek



*Název práce:*

**Vnitřní detektor ATLAS a jeho testování pomocí kosmických mionů**

*Author:* Tomáš Jakoubek

*Obor:* Jaderné inženýrství

*Druh práce:* Bakalářská práce

*Vedoucí práce:* Prom. fyz. Václav Vrba, CSc. Katedra fyziky, Fakulta jaderná a fyzikálně inženýrská, České vysoké učení technické v Praze

*Abstrakt:* V první části práce jsou nastíněny základy zatím nejúspěšnější teorie elementárních částic a jejich vzájemných interakcí, tzv. Standardního modelu. Dále jsou zde zmíněny některé teorie popisující fyziku za Standardním modelem. V druhé kapitole jsou popsány současné experimenty ve fyzice vysokých energií, zvláště Large Hadron Collider a detektor ATLAS. Výpočetní systémy určené pro zpracování dat z tohoto experimentu jsou popsány ve třetí kapitole. Pozornost je věnována především triggerovacímu systému a také tzv. Offline software. Poslední kapitola se zaměřuje na využití kosmických mionů pro testování Pixelového detektoru experimentu ATLAS. V závěru kapitoly je prezentováno několik srovnání mezi reálnými daty z měření č. 1129 a jejich Monte Carlo simulací. Shoda mezi skutečnými a nasimulovanými daty je vynikající, což ukazuje, že Pixelový detektor i software experimentu ATLAS jsou dobře připraveny na skutečná měření.

*Klíčová slova:* Standardní model, ATLAS, pixelový detektor, kosmické miony, testování.

*Title:* **ATLAS Inner Detector and its testing with Cosmic Muons**

*Author:* Tomáš Jakoubek

*Abstract:* The first chapter of this thesis presents the basics of the most successful theory of elementary particles and their interactions, the Standard Model. Also some theories beyond the Standard Model are mentioned in this part. In the second chapter the present experiments in a high energy physics are described. This section mainly concerns about the Large Hadron Collider and the ATLAS detector. The computing systems for this experiment are presented in the third chapter. The attention is mainly paid to the trigger system and the Offline software. The last chapter is concerned with using cosmic muons for the ATLAS Pixel detector testing. A comparison between real cosmic data (run 1129) and the Monte Carlo simulation is shown. Agreements between real and simulated data are excellent, which shows that the Pixel detector and the ATLAS software are well prepared to real data taking.

*Key words:* Standard Model, ATLAS, pixel detector, cosmic muons, testing.

# Contents

<b>1</b>	<b>Today's Particle Physics</b>	<b>11</b>
1.1	Basics of the Standard Model . . . . .	11
1.1.1	Particle Classification . . . . .	11
1.1.2	Leptons . . . . .	13
1.1.3	Quark Model . . . . .	15
1.1.4	Fundamental Interactions . . . . .	20
1.1.5	The Standard Model Lagrangian . . . . .	23
1.1.6	Spontaneous Symmetry Breaking . . . . .	26
1.2	Beyond the Standard Model . . . . .	28
1.2.1	Supersymmetry . . . . .	29
1.2.2	Grand Unified Theories . . . . .	29
1.2.3	Superstrings . . . . .	30
<b>2</b>	<b>High Energy Physics Experiments</b>	<b>33</b>
2.1	Why High Energies? . . . . .	33
2.2	Large Hadron Collider . . . . .	34
2.3	The ATLAS Experiment . . . . .	44
2.3.1	Inner Detector . . . . .	45
2.3.2	Calorimeters . . . . .	48
2.3.3	Muon Spectrometer . . . . .	49
2.3.4	Magnet System . . . . .	50
<b>3</b>	<b>ATLAS Computing</b>	<b>52</b>
3.1	ATLAS Trigger . . . . .	52
3.2	ATLAS Offline Software . . . . .	53
<b>4</b>	<b>Testing ATLAS Pixel Detector With Cosmic Muons</b>	<b>58</b>
4.1	Cosmic Muons . . . . .	58
4.2	Pixel EndCap Cosmic Test Setup . . . . .	59
4.3	Cosmic Data Simulation . . . . .	61
4.4	Real and Simulated Data Comparison . . . . .	62

<b>5 Thesis Summary</b>	<b>68</b>
<b>Bibliography</b>	<b>69</b>

# Chapter 1

## Today's Particle Physics

### 1.1 Basics of the Standard Model

The Standard Model is still our best describing theory of particles and their interactions. It was formulated in the 1970s and since that time it passed all experimental tests. According to this model, all matter is built from 12 fundamental fermions and their antiparticles, which interact through 3 interactions: electromagnetic, strong and weak. Fourth known interaction - gravitational - has not yet been included into the Standard Model. Basic principles of this theory will be described below in this chapter.

#### 1.1.1 Particle Classification

Fundamental particles can be divided into two groups, according to the statistics which they obey:

**Fermions** have half-integral spin ( $\frac{1}{2}\hbar, \frac{3}{2}\hbar, \dots$ ) and obey Fermi-Dirac statistics.

**Bosons** have integral spin ( $0, \hbar, 2\hbar, \dots$ ) and obey Bose-Einstein statistics.

These statistics determine how the wavefunction  $\psi$  describing an ensemble of identical particles behaves under interchange of any pair of particles. The probability

$|\psi|^2$  cannot be changed by the interchange of these particles, because they are indistinguishable. Thus, under interchange  $\psi \rightarrow \pm\psi$ . According to the *spin-statistics theorem*, following rule holds:

- under exchange of identical bosons:  $\psi \rightarrow +\psi \Rightarrow \psi$  is symmetric,
- under exchange of identical fermions:  $\psi \rightarrow -\psi \Rightarrow \psi$  is antisymmetric.

By one of effects of this rule is also *Pauli exclusion principle*: two or more identical fermions cannot exist in the same quantum state. The number of bosons in the same quantum states has no limits.

**Fermions** form “ordinary matter”. We divide them into two groups:

**Leptons** have spin  $\frac{1}{2}\hbar$  and carry integral electric charge.

**Quarks** have also spin  $\frac{1}{2}\hbar$ , but carry fractional charge (of  $+\frac{2}{3}|e|$  or  $-\frac{1}{3}|e|$ ) and form particles called hadrons.

**Bosons** are mediators for fundamental interactions:

**Electromagnetic** interaction affect particles with non-zero electric charge. For example, it bound electrons in atoms. This interaction is mediated by massless *photon* ( $\gamma$ ).

**Weak** interactions are typified by the slow process of nuclear  $\beta$ -decay. This interaction is short-range and affect particles with non-zero weak-charge. Mediators are very massive  $W^\pm$  and  $Z^0$  bosons.

**Strong** interaction affect particles with non-zero color-charge and is responsible for binding the quarks in the hadrons and also nucleons within nuclei. The interquark force is mediated by massless *gluons* ( $g$ )

**Higgs boson/s** are predicted neutral particles with zero spin, which should give masses to the intermediating bosons as well as to the other weakly interacting particles.

## Antiparticles

The relativistic relation between the total energy  $E$ , momentum  $p$  and rest mass  $m$  of the particle is

$$E^2 = p^2c^2 + m^2c^4 \quad (1.1)$$

From (1.1) we can see that the total energy  $E$  can in principle take positive as well as negative values,

$$E = \pm\sqrt{p^2c^2 + m^2c^4} \quad (1.2)$$

At first sight, negative energies for free particles look absurd. However, in quantum mechanics the amplitude of an infinite stream of particle travelling along the positive  $x$ -axis with 3-momentum  $p$  is represented by the plane wavefunction

$$\psi = Ae^{-i(ET-px)/\hbar} \quad (1.3)$$

where  $A$  is a normalisation constant. As time  $t$  increases, the phase advances in the direction of increasing  $x$ . However, (1.3) can also formally represent particle with energy  $-E$  and momentum  $-p$  travelling in the negative  $x$ -direction and backwards in time:  $Et \rightarrow (-E)(-t)$  and  $px \rightarrow (-p)(-x)$ . A stream of negatively charged particles flowing backwards in time is equivalent to positively charged particles flowing forward, and thus having  $E > 0$ . For that reason, the negative energy particle states are connected with the existence of positive energy antiparticles. Particles and antiparticles have exactly equal but opposite electrical charge and magnetic moment, other properties are identical.

Antiparticles exist for both fermions and bosons. However, for fermions there is a conservation law: the difference in the number of fermions and antifermions is a constant [1]. This implies that fermions and antifermions can only be created and destroyed in pairs.

## 1.1.2 Leptons

There are six known leptons: the electron ( $e$ ), the muon ( $\mu$ ), the tauon ( $\tau$ ) and their neutrinos. All these particles have corresponding antiparticles (such as the positron or the electron antineutrino). All known charged leptons have a single unit of negative or positive electric charge and all of the neutrinos and antineutrinos have zero electric charge. The charged leptons have two possible spin states, while only one helicity<sup>1</sup> is observed for the neutrinos (all the neutrinos are left-handed, and all the antineutrinos are right-handed). The basic properties of leptons are in Table 1.1.

**Electron** J. J. Thomson discovered the electron more than century ago and it remains the prototype of an elementary particle, while many other particles

---

<sup>1</sup>Helicity measures the sign of the component of spin of the particle,  $j_z = \pm\frac{1}{2}\hbar$ , in the direction of motion ( $z$ -direction).

discovered between then and today have lost that status. The electron is the least massive charged particle of any type. It looks to be stable, but more precisely, we just know that its mean life is  $> 4.6 \times 10^{26}$  yr. The electron has spin  $\frac{1}{2}\hbar$  and in addition to its intrinsic angular momentum, an electron has an intrinsic magnetic moment along its spin axis. When an electron collides with a positron (an antiparticle of an electron), they annihilate each other and produce pairs of high-energy photons or other particles. On the other hand, there is a process called pair production in which high-energy photons could transform into an electron and a positron, but only in the presence of a nearby charged particle, such as a nucleus.

**Muon** The negatively charged muon ( $\mu^-$ ) is like an electron, except it is more massive ( $m_\mu \doteq 207 m_e$ ). Muons are unstable, their mean life is  $2.2 \times 10^{-6}$  s. They decay to produce a virtual  $W$  boson and the matching neutrino type. The  $W$  boson then decays to produce an electron and an electron antineutrino. This decay is also an example of conservation of lepton number (see below). Because muons are much more massive than electrons, they easily pass through the electric fields inside matter with very little deflection. So, muons do not radiate and slow down as electrons do. However, they can ionize and this makes them detectable in matter.

**Tauon** The tauon is the most massive lepton ( $m_\tau \doteq 3478 m_e$ ). This third type of charged lepton is also unstable - mean life is  $2.9 \times 10^{-13}$  s. The negatively charged tauon decays to produce its matching neutrino and a virtual  $W^-$  boson. This  $W^-$  has enough energy that there are several possible ways for it to decay.

**Neutrinos** There are three known types (flavours) of neutrinos, named after their partner leptons. Neutrinos have spin  $\frac{1}{2}\hbar$  and very small mass - the Standard Model assumes that neutrinos are massless, although adding massive neutrinos to the basic framework is not difficult. Indeed, the experimentally established phenomenon of neutrino oscillation<sup>2</sup> requires neutrinos to have non-zero masses. Because neutrinos have no electric charge, they participate only in weak interaction or gravitational processes. For this reason, they are very difficult to detect.

---

<sup>2</sup>Neutrinos are most often created or detected with a well defined flavour (electron, muon, tauon). However, in a phenomenon known as neutrino flavour oscillation, neutrinos are able to oscillate between the three available flavours while they propagate through space. This may lead to break down the *lepton number conservation* (see section 1.1.2) on long enough timescales, i.e. for distances  $L$  and neutrino energies  $E$  such that  $L/E \geq 1000 \text{ m} \cdot \text{MeV}^{-1}$ .

Particle					Antiparticle					$m$ [MeV/ $c^2$ ]	$\tau$ [s]
$Q$ [ $ e $ ]	$L_e$	$L_\mu$	$L_\tau$	$Q$ [ $ e $ ]	$L_e$	$L_\mu$	$L_\tau$				
$e^-$	-1	+1	0	0	$e^+$	+1	-1	0	0	0.511	stable
$\nu_e$	0	+1	0	0	$\bar{\nu}_e$	0	-1	0	0	$< 2.2 \times 10^{-6}$	stable
$\mu^-$	-1	0	+1	0	$\mu^+$	+1	0	-1	0	105.658	$2.2 \times 10^{-6}$
$\nu_\mu$	0	0	+1	0	$\bar{\nu}_\mu$	0	0	-1	0	$< 0.17$	stable
$\tau^-$	-1	0	0	+1	$\tau^+$	+1	0	0	-1	1776.99	$2.9 \times 10^{-13}$
$\nu_\tau$	0	0	0	+1	$\bar{\nu}_\tau$	0	0	0	-1	$< 18$	stable

Table 1.1: Basic properties of leptons. Data are taken from [2].

## Lepton Numbers

Each generation of leptons shows conservation of lepton number: the sum of lepton numbers (see Tab. 1.1) in each generation must be conserved in present reaction. The first significant example of conservation of lepton number was found in the decay of the neutron. When this decay was observed, it did not fit the pattern of two-particle decay: the emitted electron does not have a definite energy as is required by conservation of energy and momentum for a two-body decay. This implied the emission of a third particle which we now identify as the electron antineutrino.

$$n \rightarrow p^+ + e^- + \bar{\nu}_e \quad (1.4)$$

The assignment of a lepton number of 1 to the electron and  $-1$  to the electron antineutrino keeps the lepton number equal to zero on both sides of the reaction above (1.4).

### 1.1.3 Quark Model

There are six different types of quark, usually known as flavours: up ( $u$ ), down ( $d$ ), charm ( $c$ ), strange ( $s$ ), top ( $t$ ) and bottom ( $b$ ). Indeed, all these particles have corresponding antiparticles. While leptons exist as free particles, quarks seem not to do so. They are confined in hadrons by the strong (or color charge) force fields. Each flavour of quark comes in three different *colors* (just a name to distinguish the three types)<sup>3</sup>. The quark forces are attractive only in “colorless” combinations of

<sup>3</sup>The total charge of the  $u$ ,  $c$ ,  $t$  quarks is  $3 \times 3 \times \frac{2}{3}|e| = 6|e|$ , that of the  $d$ ,  $s$ ,  $b$  quarks is  $-3 \times 3 \times \frac{1}{3}|e| = -3|e|$  and of the leptons is  $-3 \times 1|e| = -3|e|$ . The total charge of all the fermions is then zero. This is the actual condition that the Standard Model should be free of so-called “anomalies” and is a renormalisable field theory.

three quarks (baryons), quark-antiquark pairs (mesons) and possibly larger combinations such as the pentaquark that could also meet the colorless condition. Quarks have spin  $\frac{1}{2}\hbar$  and, by convention, positive parity (antiquarks have negative parity). The additive baryon number ( $\mathcal{B}$ ) of quarks is  $\frac{1}{3}$  and of antiquarks  $-\frac{1}{3}$ . The relation between the other additive quantum numbers (denoted by the initial of the quark name  $S, C, B, T$ ) and charge  $Q$  is

$$Q = I_z + \frac{\mathcal{B} + S + C + B + T}{2} \quad (1.5)$$

The last quantum number is hypercharge and is defined as

$$Y = \mathcal{B} + S \quad (1.6)$$

In strong interactions between the quarks, the flavour quantum number is conserved. In fact, quarks may change flavour, in such a way that  $\Delta S = \pm 1$ ,  $\Delta C = \pm 1$  etc., but this is only possible for a weak interaction. Basic properties of quarks are in Tab. 1.2.

	$m$ [GeV/ $c^2$ ]	$Q$ [[e]]	$I_z$	$S$	$C$	$B$	$T$
$d$	$(3.0 \div 7.0) \times 10^{-3}$	$-\frac{1}{3}$	$-\frac{1}{2}$	0	0	0	0
$u$	$(1.5 \div 3.0) \times 10^{-3}$	$+\frac{2}{3}$	$+\frac{1}{2}$	0	0	0	0
$s$	$(95 \pm 25) \times 10^{-3}$	$-\frac{1}{3}$	0	-1	0	0	0
$c$	$1.25 \pm 0.09$	$+\frac{2}{3}$	0	0	+1	0	0
$b$	$4.20 \pm 0.07$	$-\frac{1}{3}$	0	0	0	-1	0
$t$	$174.2 \pm 3.3$	$+\frac{2}{3}$	0	0	0	0	+1

Table 1.2: Properties of quarks. Data are taken from [2].

## Weight Diagrams

Using the  $SU(3)$  symmetry, the fundamental representatoin of the quark is the triplet (denoted  $\mathbf{3}$ )

$$q = \begin{pmatrix} u \\ d \\ s \end{pmatrix} \quad (1.7)$$

The  $SU(3)$  contains subgroups  $SU(2)$  of isospin and  $U(1)$  of hypercharge. Members of the quark triplet can be plotted into diagram, where the hypercharge  $Y$  is on the vertical axis and the third componet of isospin  $I_z$  on the horizontal axis. The weight diagrams of the quark and antiquark triplets are on the Fig. 1.1.

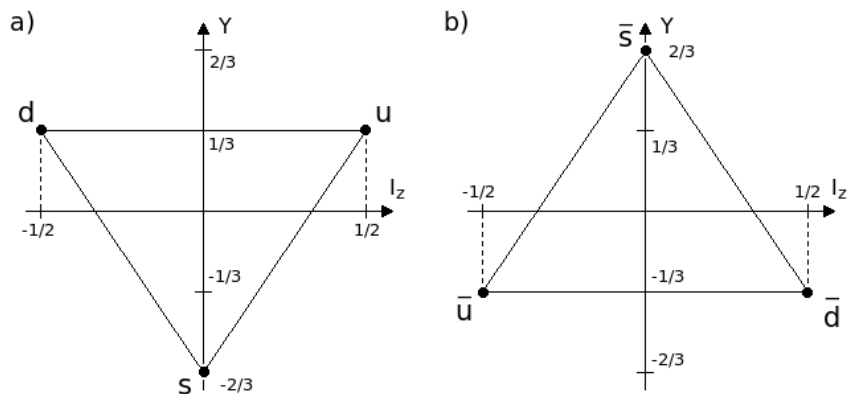


Figure 1.1: Weight diagram for a) the triplet  $\mathbf{3}$ , b) the antitriplet  $\bar{\mathbf{3}}$ .

**Mesons** are bound states of quarks  $q$  and antiquarks  $\bar{q}$  (flavour of  $q$  can be different from flavour of  $\bar{q}$ ). Thus they have baryon number  $\mathcal{B} = 0$ . The parity is defined as  $P = (-1)^{l+1}$  where  $l$  is the orbital angular momentum of the  $q\bar{q}$  state. Spin  $J$  is given by the relation  $|l - s| < J < |l + s|$  where  $s = 0$  for antiparallel quark spins or  $s = 1$  for parallel quark spins. The charge conjugation  $C = (-1)^{l+s}$  is defined only for mesons made of quark and its own antiquark. Now, we can sort the mesons in so called  $J^{PC}$  multiplets:

- for  $l = 0$  states as the pseudoscalars ( $0^{-+}$ ) and the vectors ( $1^{--}$ )
- for  $l = 1$  as the scalars ( $0^{++}$ ), the axial vectors ( $1^{++}$  and  $1^{+-}$ ) and the tensors ( $2^{++}$ ).

The *natural spin-parity* series is formed by those mesons where  $P = (-1)^J$ . According to the above, they must have  $s = 1$  and hence  $CP = +1$ . Mesons with natural spin-parity and  $CP = -1$  (e. g.  $0^{+-}$ ,  $1^{-+}$ ,  $2^{+-}$ ,  $3^{-+}$ , etc.) are forbidden in this model. The  $J^{PC} = 0^{- -}$  state is forbidden as well. However, mesons with these “forbidden” quantum numbers may exist, but would lie outside the presented model [2].

As the product of representations of the  $SU(3)$  we get the nine possible  $q\bar{q}$  combinations containing the  $u$ ,  $d$  and  $s$  quarks. To satisfy the conditions of irreducible<sup>4</sup> representations, we decompose this direct product into an octet and a singlet<sup>5</sup>:

$$\mathbf{3} \otimes \bar{\mathbf{3}} = \mathbf{8} \oplus \mathbf{1} \quad (1.8)$$

<sup>4</sup>If it is possible to decompose some representation of the group into a direct sum of other independent representations, we call them “reducible”. If not, we call them “irreducible”.

<sup>5</sup>These decompositions are well-described by the Yang tableaux (see [4] for more information). In the simple cases we can use graphical method and relations  $\mathbf{N} \otimes \bar{\mathbf{N}} = (\mathbf{N}^2 - 1) \oplus \mathbf{1}$  and  $\mathbf{N} \otimes \mathbf{N} = \frac{N(N-1)}{2} \oplus \frac{N(N+1)}{2}$  [4].

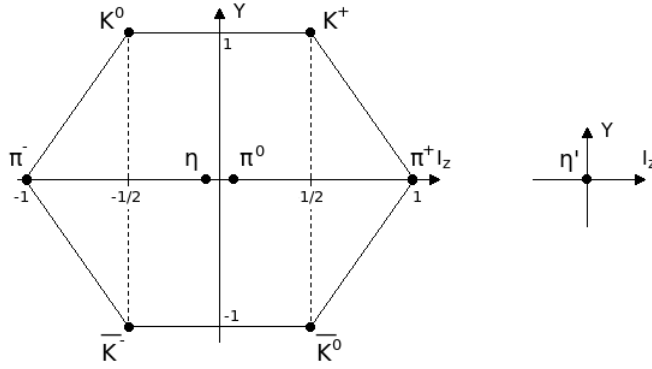


Figure 1.2: Weight diagram for  $0^-$  meson (octet  $\mathbf{8}$  and singlet  $\mathbf{1}$ )

The weight diagram for  $J^P = 0^-$  pseudoscalar meson is on the Fig. 1.2.

A fourth quark such as charm  $c$  can be included by extending  $SU(3)$  symmetry to  $SU(4)$ . However,  $SU(4)$  is “badly broken”, because of the much heavier  $c$  quark. Nevertheless, in an  $SU(4)$  classification the sixteen mesons are grouped into a 15-plet and a singlet:

$$\mathbf{4} \otimes \bar{\mathbf{4}} = \mathbf{15} \oplus \mathbf{1} \quad (1.9)$$

The weight diagrams for the ground-state pseudoscalar ( $J^{PC} = 0^{-+}$ ) and vector ( $J^{PC} = 1^{-}$ ) mesons are shown on the Fig. 1.3.

**Baryons** are composed of three<sup>6</sup> quarks, so they have baryon number  $\mathcal{B} = 1$ . The “ordinary” baryons are made up of  $u$ ,  $d$  and  $s$  quarks. Because of their three possible flavours they must belong to the multiplets on the right side of

$$\mathbf{3} \otimes \mathbf{3} \otimes \mathbf{3} = \mathbf{10}_S \oplus \mathbf{8}_M \oplus \mathbf{8}_M \oplus \mathbf{1}_A \quad (1.10)$$

where the subscripts indicate symmetric, mixed-symmetry, or antisymmetric states under interchange of any two quarks. The mechanism is the same as for the mesons (see above). Examples of the weight diagrams for  $\frac{1}{2}^+$  baryon octet  $\mathbf{8}$  and  $\frac{3}{2}^+$  baryon decuplet  $\mathbf{10}$  you can see on the Fig. 1.4.

It is possible to extend the flavour symmetry to  $SU(4)$  by adding the  $c$  quark to the group of  $u$ ,  $d$  and  $s$  quarks. However, because of the large mass of the  $c$  quark, this symmetry is strongly broken as with mesons  $SU(4)$ . On the Fig. 1.5 you can see the  $SU(4)$  baryon multiplets that have as their bottom

<sup>6</sup>In the most general case, baryons are composed of three quarks plus any number of quark - antiquark pairs. Although recently some experimental evidence for  $(qqqq\bar{q})$  pentaquark states has been claimed, so far all established baryons are 3-quark  $(qqq)$  configurations [2].

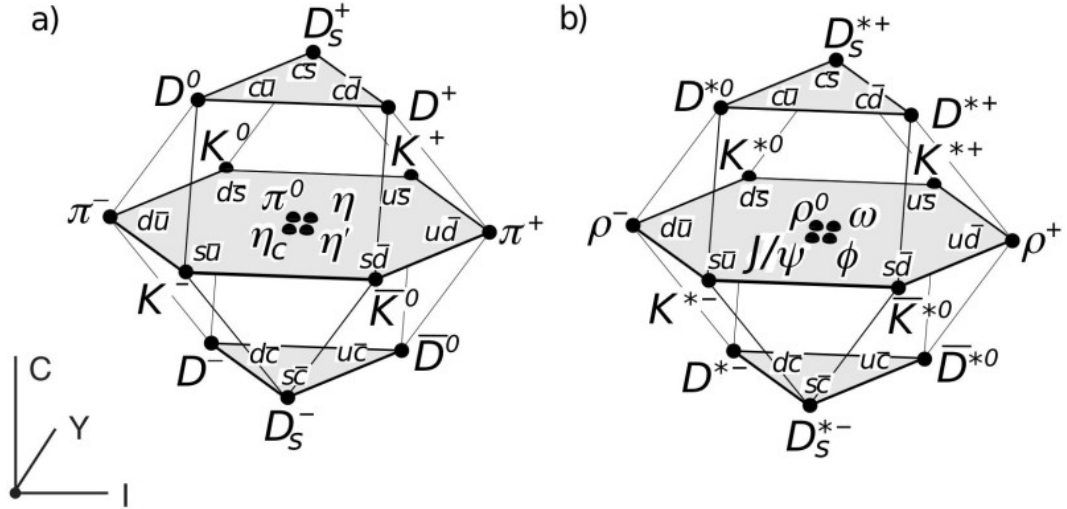


Figure 1.3:  $SU(4)$  weight diagram showing the 16-plets for the pseudoscalar (a) and vector (b) mesons made of the  $u$ ,  $d$ ,  $s$  and  $c$  quarks as a function of isospin  $I$ , charm  $C$  and hypercharge  $Y = B + S - \frac{C}{3}$ . Figure from [2].

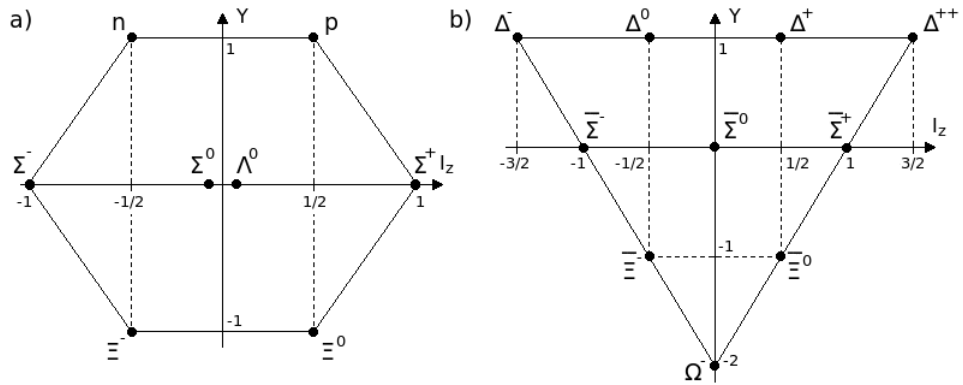


Figure 1.4: Weight diagram for a)  $\frac{1}{2}^+$  baryon octet **8**, b)  $\frac{3}{2}^+$  baryon decuplet **10**

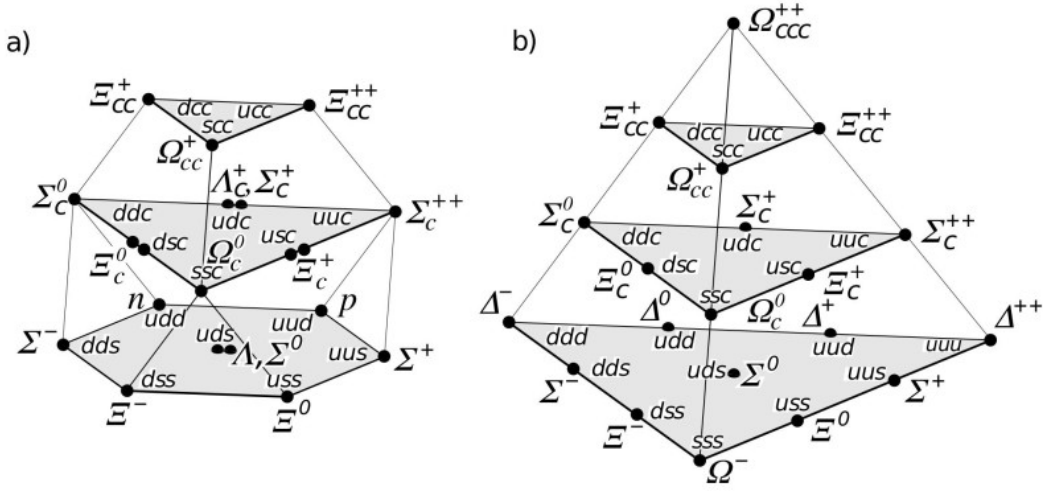


Figure 1.5:  $SU(4)$  multiplets of baryons made of  $u$ ,  $d$ ,  $s$ , and  $c$  quarks; a) The 20-plet with an  $SU(3)$  octet, b) the 20-plet with an  $SU(3)$  decuplet. Figure from [2].

levels an  $SU(3)$  octet, such as the octet that includes the nucleon, or an  $SU(3)$  decuplet, such as the decuplet that includes the  $\Delta(1232)$ .

### 1.1.4 Fundamental Interactions

**Electromagnetic Interaction** The Electromagnetic interaction is well described by *quantum electrodynamics* ( $QED$ ) which is the gauge theory having the Abelian  $U(1)$  symmetry. The symmetry of interaction is described by one free parameter which corresponds to one intermediate particle (photon  $\gamma$ ).

The EM interaction is selective - affects only particles with non-zero electric charge, and has infinite range. This corresponds to zero mass of photon - if the interaction is supposed to have an infinite range, the mediators have to be massless.

The strength of EM interaction is specified by the dimensionless coupling constant

$$\alpha = \frac{e^2}{4\pi\hbar c} \approx \frac{1}{137} \quad (1.11)$$

This quantity is called *the fine structure constant*, because it determines the fine structure (spin-orbit splitting) in atomic spectra.

On the Fig. 1.6 you can see so-called *Feynman diagrams* of typical EM processes:  $e^-e^-$  scattering (a) and Compton scattering (b). Particles are represented by lines with arrows to denote the direction of their travel, antiparticles

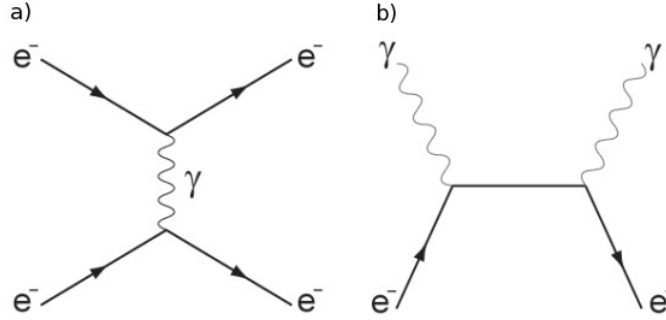


Figure 1.6: Feynman diagrams of a)  $e^-e^-$  scattering, b) Compton scattering. Figures from [16] and [17].

have their arrows reversed. Virtual particles are represented by wavy (or broken) lines and have no arrows. Only lines entering or leaving the diagram represent observable particles. The amplitude of probability correspond to the number of vertices. This probability is proportional to the fine structure constant  $\alpha$  and decreases with every extra vertex.

**Strong Interaction** As the EM interaction is described by *QED*, the strong interaction is formulated in the non-Abelian gauge theory with  $SU(3)$  color symmetry which is called *quantum chromodynamics (QCD)*. The symmetry is described by the unitary complex matrices  $3 \times 3$  which contains 9 elements. However, the condition of  $\det = 1$  decreases the number of free parameters to 8 which correspond to 8 intermediate particles (gluons  $g$ ).

The strong interaction affects only particles with non-zero color-charge. However the gluons are massless, the range of interaction is finite (of order  $10^{-15}$  m). That is probably because of screening of the color field.

The coupling constant of the strong interaction is

$$\alpha_s = \frac{g_s^2}{4\pi} \approx 1 \quad (1.12)$$

where  $g_s$  is the strong charge of the constituent quarks. However,  $\alpha_s$  behaves like function of the 4-momentum transfer square ( $q^2$ ):

$$\alpha_s(q^2) = \frac{\alpha_s(q_0^2)}{1 + \frac{7}{4\pi}\alpha_s(q_0^2) \ln\left(\frac{q^2}{q_0^2}\right)} \quad (1.13)$$

From (1.13), it is obvious that at asymptotically large  $q^2$ , the coupling  $\alpha_s(q^2) \rightarrow 0$ , i.e. the quarks behave as if free. That phenomenon is known as *asymptotic*

*freedom*. On the other hand, at small  $q^2$ , as in the state of bound quarks, the  $\alpha_s$  becomes large. That is called *confinement phase*.

On the Fig. 1.7 you can see Feynman diagram of a strong proton-neutron interaction mediated by a neutral pion ( $\pi^0$ ).

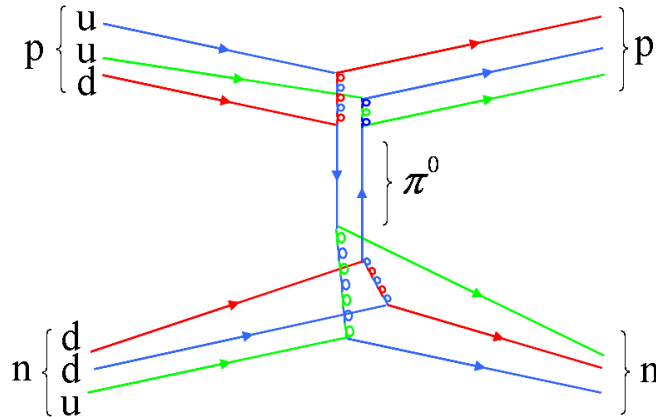


Figure 1.7: A Feynman diagram of a strong proton-neutron interaction mediated by a neutral pion ( $\pi^0$ ). Individual quark constituents are shown to illustrate how the strong interaction gives rise to the nuclear force. Straight lines are quarks and multi-colored loops are gluons. Other gluons which bind together the proton, neutron, and pion “in-flight”, are not shown. Figure from [15].

**Weak Interaction** The theory of weak interactions for weak processes was developed in 1950s and works well for low energy processes. However, the theory is not renormalizable in spite of its small coupling constant. This is due to the fact that the Fermi coupling  $G_F$  has the dimension of  $(mass)^{-2}$  (and for  $mc^2 = 1$  GeV is  $G_F \approx 1.17 \times 10^{-5}$  GeV $^{-2}$ ). A renormalizable theory was finally formulated, based on the unified picture of weak and electromagnetic interactions, in the framework of non-Abelian gauge theory with  $SU(2) \times U(1)$  symmetry which is now called the electroweak standard model. This symmetry is described by the unitary complex matrices  $2 \times 2$ . The condition of  $\det = 1$  decreases the number of free parameters to 3 which correspond to 3 intermediate particles:  $W^+$ ,  $W^-$  and  $Z^0$ .

The weak interaction affects only particles with non-zero weak-charge (flavour). Because intermediate bosons are very massive ( $m_{W^\pm} \doteq 80.4$  GeV,  $m_{Z^0} \doteq 91.2$  GeV [2]), the range of interaction is finite (of order  $10^{-17}$  m).

On the Fig. 1.8 you can see Feynman diagram of a typical weak process:  $\beta$ -decay of a neutron  $n \rightarrow p^+ + e^- + \bar{\nu}_e$ .

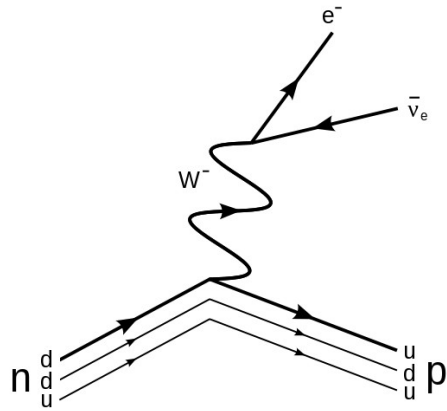


Figure 1.8: A Feynman diagram of a typical weak process:  $\beta$ -decay of a neutron ( $n$ ) into a proton ( $p$ ), electron ( $e^-$ ), and electron antineutrino ( $\bar{\nu}_e$ ) via an intermediate  $W^-$  boson. Figure from [14].

Weak and EM interactions are described by the gauge theory with  $SU(2) \times U(1)$  symmetry and the strong interaction is formulated by the gauge theory with  $SU(3)$  symmetry. Therefore, we can expect that all these interactions must be described by the gauge theory with some internal symmetry  $G$ . The simplest way to make the symmetry group  $G$  is as a direct product of each symmetry:  $G = SU(3) \times SU(2) \times U(1)$ . That is what we call the Standard Model.

### 1.1.5 The Standard Model Lagrangian

As the other physical theories, also the Standard Model of particle physics is formulated using the *Lagrange formalism*. However, the whole theory (including *QCD* and *QED*) is too complex to be exactly described in this thesis. Thus only basic statements and results will be shown. More information can be found e.g. in books [8] or [9]. The following description of the Standard Model Lagrangian is divided into two sections (*QCD* and *QED* part).

**The strong interaction part** (*QCD*) of the theory is described by the Lagrangian

$$\mathcal{L}_{QCD} = -\frac{1}{4}F_{\mu\nu}^i F^{i\mu\nu} + \sum_r \bar{q}_{r\alpha} i \not{D}_\beta^\alpha q_r^\beta \quad (1.14)$$

where

$$F_{\mu\nu}^i = \partial_\mu G_\nu^i - \partial_\nu G_\mu^i - g_s f_{ijk} G_\mu^j G_\nu^k \quad (1.15)$$

is the field strength tensor for the gluon fields  $G_\mu^i$ ,  $i = 1, \dots, 8$ , with the *QCD*

gauge coupling constant  $g_s$ . The structure constants  $f_{ijk}$  ( $i, j, k = 1, \dots, 8$ ) are defined by

$$[\lambda^i, \lambda^j] = 2if_{ijk}\lambda^k \quad (1.16)$$

where the  $SU(3)$   $\lambda$  matrices are defined in Tab. 1.3. The second part of (1.14) is the gauge covariant derivative for the quarks:  $q_r$  is the  $r^{\text{th}}$  quark flavor,  $\alpha, \beta = 1, 2, 3$  are color indices, and

$$D_{\mu\beta}^\alpha = (D_\mu)_{\alpha\beta} = \partial_\mu \delta_{\alpha\beta} + ig_s G_\mu^i L_{\alpha\beta}^i \quad (1.17)$$

where the quarks transform according to the triplet representation matrices  $L^i = \frac{\lambda^i}{2}$ .

Although  $QCD$  allows mass terms in Lagrangian, these are forbidden by the chiral symmetry of the electroweak part of the theory (see below). That is the reason for generating quark masses by *spontaneous symmetry breaking* (see section 1.1.6).

$$\begin{array}{lll} \lambda^1 = \begin{pmatrix} 0 & 1 & 0 \\ 1 & 0 & 0 \\ 0 & 0 & 0 \end{pmatrix} & \lambda^2 = \begin{pmatrix} 0 & -i & 0 \\ i & 0 & 0 \\ 0 & 0 & 0 \end{pmatrix} & \lambda^3 = \begin{pmatrix} 1 & 0 & 0 \\ 0 & -1 & 0 \\ 0 & 0 & 0 \end{pmatrix} \\ \lambda^4 = \begin{pmatrix} 0 & 0 & 1 \\ 0 & 0 & 0 \\ 1 & 0 & 0 \end{pmatrix} & \lambda^5 = \begin{pmatrix} 0 & 0 & -i \\ 0 & 0 & 0 \\ i & 0 & 0 \end{pmatrix} & \lambda^6 = \begin{pmatrix} 0 & 0 & 0 \\ 0 & 0 & 1 \\ 0 & 1 & 0 \end{pmatrix} \\ \lambda^7 = \begin{pmatrix} 0 & 0 & 0 \\ 0 & 0 & -i \\ 0 & i & 0 \end{pmatrix} & \lambda^8 = \frac{1}{\sqrt{3}} \begin{pmatrix} 1 & 0 & 0 \\ 0 & 1 & 0 \\ 0 & 0 & -2 \end{pmatrix} & \end{array}$$

Table 1.3: The Gell-Mann matrices  $\lambda^i$  are generators of the  $SU(3)$  group.

**The electroweak theory** is based on the  $SU(2) \times U(1)$  Lagrangian

$$\mathcal{L}_{QED} = \mathcal{L}_{gauge} + \mathcal{L}_{Higgs} + \mathcal{L}_{fermion} + \mathcal{L}_{Yukawa} \quad (1.18)$$

The gauge part is

$$\mathcal{L}_{gauge} = -\frac{1}{4}F_{\mu\nu}^i F^{\mu\nu i} - \frac{1}{4}B_{\mu\nu} B^{\mu\nu} \quad (1.19)$$

with field strength tensors

$$\begin{aligned} B_{\mu\nu} &= \partial_\mu B_\nu - \partial_\nu B_\mu \\ F_{\mu\nu} &= \partial_\mu W_\nu^i - \partial_\nu W_\mu^i - g\epsilon_{ijk} W_\mu^j W_\nu^k \end{aligned} \quad (1.20)$$

where  $W_\mu^i, i = 1, 2, 3$  and  $B_\mu$  are respectively the  $SU(2)$  and  $U(1)$  gauge fields,  $g$  is the  $SU(2)$  gauge coupling and  $\epsilon_{ijk}$  is the totally antisymmetric symbol. These terms contain the kinetic energy of the gauge fields and their self interactions.

The scalar part of Lagrangian contains the kinetic energy of the Higgs field, its gauge interactions and the Higgs potential:

$$\mathcal{L}_{Higgs} = (D^\mu \varphi)^\dagger D_\mu \varphi - V(\varphi) \quad (1.21)$$

where  $\varphi = \begin{pmatrix} \varphi^+ \\ \varphi^0 \end{pmatrix}$  is a complex Higgs scalar,

$$V(\varphi) = \mu^2 \varphi^\dagger \varphi + \lambda (\varphi^\dagger \varphi)^2 \quad (1.22)$$

is the Higgs potential with  $\lambda > 0$ , and the gauge covariant derivative is defined as

$$D_\mu \varphi = \left( \partial_\mu + \frac{ig}{2} \sigma^i W_\mu^i + \frac{ig'}{2} B_\mu \right) \varphi \quad (1.23)$$

where the  $\sigma^i$  are the Pauli matrices

$$\sigma^1 = \begin{pmatrix} 0 & 1 \\ 1 & 0 \end{pmatrix}, \quad \sigma^2 = \begin{pmatrix} 0 & -i \\ i & 0 \end{pmatrix}, \quad \sigma^3 = \begin{pmatrix} 1 & 0 \\ 0 & -1 \end{pmatrix} \quad (1.24)$$

and  $g'$  is the  $U(1)$  gauge coupling. For  $\mu^2 < 0$  in (1.22) there will be mentioned spontaneous symmetry breaking.

The fermion term is

$$\mathcal{L}_{fermion} = \sum_{m=1}^N (\bar{q}_{mL}^0 i \not{D} q_{mL}^0 + \bar{l}_{mL}^0 i \not{D} l_{mL}^0 + \bar{u}_{mR}^0 i \not{D} u_{mR}^0 + \bar{d}_{mR}^0 i \not{D} d_{mR}^0 + \bar{e}_{mR}^0 i \not{D} e_{mR}^0) \quad (1.25)$$

where  $m$  is the family index,  $N \geq 3$  is the number of families and  $L/R$  indices refer to the left/right chiral projections. The quark color indices  $\alpha = r, g, b$  have been suppressed. This piece of Lagrangian contains the kinetic energy of the fermions and their interactions with the gauge fields which are contained in the covariant derivatives

$$\begin{aligned} D_\mu q_{mL}^0 &= \left( \partial_\mu + \frac{ig}{2} \sigma^i W_\mu^i + \frac{ig'}{6} B_\mu \right) q_{mL}^0 \\ D_\mu l_{mL}^0 &= \left( \partial_\mu + \frac{ig}{2} \sigma^i W_\mu^i - \frac{ig'}{2} B_\mu \right) l_{mL}^0 \end{aligned}$$

$$\begin{aligned}
D_\mu u_{mR}^0 &= \left( \partial_\mu + 2\frac{ig'}{3}B_\mu \right) u_{mR}^0 \\
D_\mu d_{mR}^0 &= \left( \partial_\mu - \frac{ig'}{3}B_\mu \right) d_{mR}^0 \\
D_\mu e_{mR}^0 &= (\partial_\mu - ig'B_\mu) e_{mR}^0
\end{aligned} \tag{1.26}$$

The different transformations of the  $L$  and  $R$  fields (i.e. the symmetry is chiral) is the origin of parity violation in the electroweak sector. The chiral symmetry also forbids any bare mass terms for the fermions.

The last term in (1.18) is

$$\mathcal{L}_{Yukawa} = - \sum_{m,n=1}^F [\Gamma_{mn}^u \bar{q}_{mL}^0 \tilde{\varphi} u_{mR}^0 + \Gamma_{mn}^d \bar{q}_{mL}^0 \varphi d_{nR}^0 + \Gamma_{mn}^e \bar{l}_{mn}^0 \varphi e_{nR}^0] + \text{h.c.} \tag{1.27}$$

where the matrices  $\Gamma_{mn}$  describe the Yukawa couplings between the single Higgs doublet (these matrices contain most of the parameters of the Standard Model) and the various flavors  $m$  and  $n$  of quarks and leptons.

### 1.1.6 Spontaneous Symmetry Breaking

As it was mentioned in the previous section, gauge invariance does not allow mass terms in the Lagrangian for the gauge bosons. However massless gauge bosons are not acceptable for the weak interaction which is known to be short-ranged. That means the gauge invariance must be broken spontaneously which preserves the renormalizability. The idea is simply that the lowest energy (vacuum) state does not respect the gauge symmetry and induces effective masses for particles propagating through it.

To find a minimum of the Higgs potential (1.22), we define a new real variable  $\rho^2 = \varphi^\dagger \varphi$ . Thus (1.22) becomes

$$V(\rho) = \mu^2 \rho^2 + \lambda \rho^4 \tag{1.28}$$

which must be minimized with respect to  $\rho$ :

$$V'(\rho) = 2\rho(\mu^2 + 2\lambda\rho^2) = 0 \tag{1.29}$$

Two important cases are illustrated on the Fig. 1.9. For  $\mu^2 > 0$  the minimum occurs at  $\rho = 0$ . That is, the vacuum is empty space and  $SU(2) \times U(1)$  is unbroken at the

minimum. For  $\mu^2 < 0$  the  $\rho = 0$  symmetric point is unstable, and the minimum occurs at  $\rho = \pm\mu/\sqrt{2\lambda}$  which breaks the  $SU(2) \times U(1)$  symmetry. Returning to the original variable  $\varphi$  we obtain a continuous one-parameter set of constant fields

$$\varphi_0 = \frac{v}{\sqrt{2}}e^{i\alpha} \quad (1.30)$$

where  $v = \mu/\lambda$  so-called “vacuum” and  $\alpha$  is an arbitrary real parameter. This relation fixes a notation that has become standard for electroweak theories involving *Higgs mechanism*.

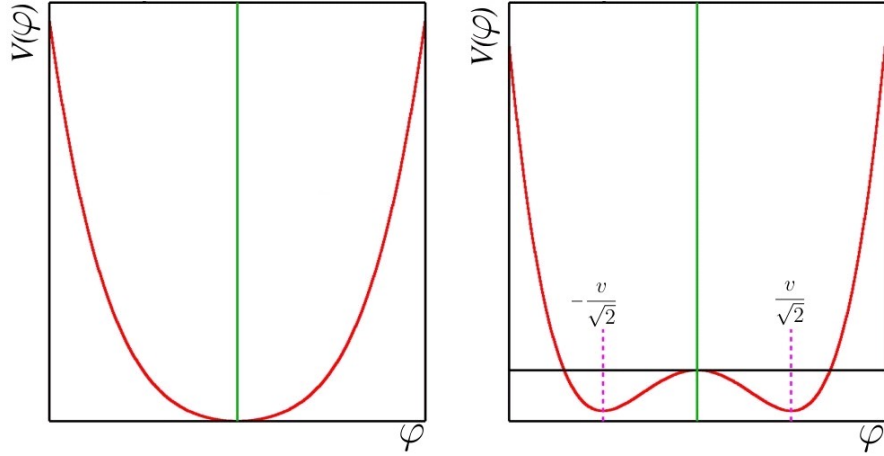


Figure 1.9: The Higgs potential  $V(\varphi)$  for  $\mu^2 > 0$  (left) and  $\mu^2 < 0$  (right). Figure from [18].

To display the physical particle content it is useful to go to the unitary gauge, in which the scalar covariant kinetic energy term in (1.21) takes the form

$$(D_\mu\varphi)^\dagger D^\mu\varphi \rightarrow M_W^2 W^{+\mu}W_\mu^- + \frac{M_Z^2}{2} Z^\mu Z_\mu + H \text{ terms} \quad (1.31)$$

where  $H$  is a Hermitian field which will turn out to be the physical Higgs scalar (the kinetic energy and gauge interaction terms of this scalar have been omitted). Thus, spontaneous symmetry breaking generates mass terms for the  $W$  and  $Z$  gauge bosons

$$\begin{aligned} W^\pm &= \frac{1}{\sqrt{2}}(W^1 \mp iW^2) \\ Z &= -\sin\theta_W B + \cos\theta_W W^3 \end{aligned} \quad (1.32)$$

The masses are

$$M_W = \frac{gv}{2} \quad (1.33)$$

and

$$M_Z = \frac{v}{2} \sqrt{g^2 + g'^2} = \frac{M_W}{\cos \theta_W} \quad (1.34)$$

where the weak angle is defined by  $\tan \theta_W \equiv g'/g$ . [6]

The Yukawa interaction in the unitary gauge becomes

$$-\mathcal{L}_{Yukawa} \rightarrow \bar{u}_L^0 (M^u + h^u H) u_R^0 + (d, e) \text{ terms} + \text{h.c.} \quad (1.35)$$

where  $u_L^0$  and  $u_R^0$  are an  $N$ -component column vectors,  $M^u$  is an  $N \times N$  fermion mass matrix  $M_{mn}^u = \Gamma_{mn}^u v / \sqrt{2}$  induced by spontaneous symmetry breaking, and  $h^u = M^u / v = gM^u / 2M_W$  is the Yukawa coupling matrix. In general  $M$  is not diagonal, Hermitian, or symmetric. To identify the physical particle content it is necessary to diagonalize  $M$  by separate unitary transformations  $A_L$  and  $A_R$  on the left- and right-handed fermion fields. [6]

## 1.2 Beyond the Standard Model

While the Standard Model provides a very good description of phenomena observed by experiments, it is still an incomplete theory - there are number of shortcomings and problems. Attempts have been made to carry unification further, by combining the electroweak and strong interactions in a higher, unified symmetry which could be manifest at extremely high energy. The scale of so-called “grand unified theories” ( $GUT$ ) is believed to be  $E_{GUT} \sim 10^{16}$  GeV.

Once, however, one admits to the possibility of higher mass scales - and we already know, for example, that a typical gravitational mass scale where quantum effects could be important is the Planck scale at  $10^{19}$  GeV - difficulties start to arise for the Standard Model. This is called “hierarchy problem”. If there are much more massive particles  $M \simeq M_{GUT}$  in the unexplored region above the electroweak mass scale of  $M_W \sim G^{-1/2}$ , these will inevitably occur in virtual processes at lower energy scales. If the mass of the (electroweak) Higgs particle (i.e. its self-energy) is driven by the more massive Higgs objects of the  $GUT$  scale, its value will become unstable (i.e. divergent), unless we can arrange clever and quite precise cancellations at the level of  $M_W / M_{GUT} \simeq 10^{-14}$ . *Supersymmetric models* are designed to do just that.

### 1.2.1 Supersymmetry

This hypothesis can solve the hierarchy problem mentioned above. It postulates a fermion-boson symmetry, according to which new fermion (boson) partners are postulated for all known fundamental bosons (fermions). Of course this symmetry cannot be exact, otherwise the superpartners would have the same mass as the original particles which is clearly not the case. The superpartners are heavier than the known elementary particles. Experiments carried out so far have not had particle beams of sufficient energy and intensity to produce them in observable numbers.

Unfortunately, current theoretical ideas are insufficient to accurately predict the superpartner masses, though the way in which these particles interact with one another and with the known particles is predicted precisely. Even though accurate predictions of the the superpartner masses do not exist, there are three distinct arguments that make qualitative predictions of the masses. All three of them lead to the conclusion that a typical superpartner mass should be in the range of  $100 \div 1000$  GeV.

It is generally assumed that *SUSY* particles would be produced in association, with conservation of a special quantum number  $R$ , i.e. in pairs with  $R = \pm 1$ . For example, a squark-antisquark pair (the squark is a superpartner to quark) can be produced in quark-antiquark annihilation:  $q + \bar{q} \rightarrow \tilde{q} + \tilde{\bar{q}}$ .

The most widely quoted scheme is that of the Minimal Supersymmetric Standard Model (*MSSM*). Examples of the superparticles in this model are in Tab. 1.4. In *SUSY* models a minimum of two complex Higgs doublets are required, yielding eight components in all and five physical Higgs particles. In addition, one expects superpartners, the spin  $\frac{1}{2}\hbar$  Higgsinos ( $H_{1,2}^0, H^\pm$ ). The gauginos ( $\tilde{\gamma}, \tilde{W}^\pm, \tilde{Z}^0$ ) mix with the Higgsinos to form four mass eigenstates called “charginos” ( $\chi_{1,2}^\pm$ ) and four called “neutralinos” ( $\chi_{1,2,3,4}^0$ ).

### 1.2.2 Grand Unified Theories

The success of the electroweak model, unifying weak and electromagnetic interaction, opened the possibility that the strong interactions might also be included in a unifying scheme. The basic idea is that the  $SU(2) \times U(1)$  electroweak symmetry and the  $SU(3)$  colour symmetry of the strong interactions might be encompassed

Particle	Spin	S-particle	Spin
quark $q$	$\frac{1}{2}$	squark $\tilde{q}$	0
lepton $l$	$\frac{1}{2}$	slepton $\tilde{l}$	0
photon $\gamma$	1	photino $\tilde{\gamma}$	$\frac{1}{2}$
gluon $g$	1	gluino $\tilde{g}$	$\frac{1}{2}$
$W^\pm$	1	wino $\tilde{W}^\pm$	$\frac{1}{2}$
$Z^0$	1	zino $\tilde{Z}^0$	$\frac{1}{2}$

Table 1.4: Particles and their *SUSY* partners.

by a more global symmetry at some high unification energy, well above the electroweak scale.

The couplings of the various interactions “run” in different ways. The coupling of  $U(1)$  increases with energy, while the couplings of  $SU(2)$  and  $SU(3)$  decrease with increasing energy. If we assume that there is no new physics between the electroweak scale and that of grand unification, is it possible to extrapolate these couplings to a common value at some unknown energy, where the coupling would be universal?

There are many ways in which all three symmetries might be incorporated into a more global symmetry. The first and simplest *GUT* model was the  $SU(5)$  model of Georgi and Glashow. This incorporates the known fermions (both the leptons and the quarks) into multiplets, inside which, having the same universal coupling, leptons and quarks can transform one into the other. They interact via the mediation of massive bosons  $X$  and  $Y$ , with electric charges  $-\frac{4}{3}|e|$  and  $-\frac{1}{3}|e|$  respectively. These carry three colours and, counting both particles and antiparticles, therefore exist in 12 varieties. Including the eight gluons of  $SU(3)$  and the  $W^\pm$ ,  $Z^0$  and  $\gamma$  of  $SU(2)$  and  $U(1)$ , there are a total of 24 gauge bosons.

### 1.2.3 Superstrings

Many attempts have been made to incorporate a renormalisable field theory of gravity along with the other fundamental interactions into a single model. The basic problem for a quantum field theory of gravity is that literally pointlike interactions lead to incurable divergences. This is overcome by replacing the point particles by *strings* of finite length. Since the only naturally occurring length in gravity is the Planck length, the strings are expected to have dimensions of this

order

$$l_P = \sqrt{\frac{\hbar G_N}{c^3}} = 1.6 \times 10^{-35} \text{ m} \quad (1.36)$$

Elementary particles can be represented as closed strings with the different particles corresponding to different modes of oscillation of the loop. The theory, in order to be renormalisable, has to be formulated in 10 or more dimensions, all but the normal four space-time dimensions being “curled up” or compacted within size  $l_P$  and hence undetectable. Although originally formulated in connection with strong interactions, it was found early on that the graviton, the (still hypothetical) massless spin  $2\hbar$  mediator of the gravitational field, occurred naturally in the supersymmetric version of the theory.

The known elementary particles are associated with string excitations of lowest, i.e. effectively zero, mass compared with  $M_P = 1.2 \times 10^{19}$  GeV, and include those of spin  $J = 0, \frac{1}{2}, 1, \frac{3}{2}$  and 2 (in terms of  $\hbar$ ), to be identified possibly with Higgs scalars, quarks, leptons, gauge bosons and, most importantly, a graviton of spin  $2\hbar$  and its *SUSY* partner, the gravitino of spin  $\frac{3}{2}\hbar$ . An important feature of string theory in general is that closed strings representing the conventional elementary particles are not the only topologies that are possible. In grand unified theories, the strings can be identified with the lines of the gauge field.  $W$ 's,  $Z$ 's etc. correspond to simple closed loops which can disappear by decay. However, they can interact with each other and the strings can get tangled up in knots which are permanent.



# Chapter 2

## High Energy Physics Experiments

### 2.1 Why High Energies?

There are at least three reasons why high energy accelerators are needed for particles physics experiments. The first two of them have connection with studying elementary particles. The word *elementary* is used in the sense that such particles have no known structure - they are pointlike. The question is “How pointlike is pointlike?” It depends of the spatial resolution of the “microscope” which is used. In an optical microscope, the resolution is

$$\Delta r \simeq \frac{\lambda}{\sin \theta} \quad (2.1)$$

where  $\theta$  is the angular aperture of the light beam used to view the object and  $\lambda$  is the wavelength. Substituting the de Broglie relation  $\lambda = h/p$ , the resolution becomes

$$\Delta r \simeq \frac{\lambda}{\sin \theta} = \frac{h}{p \sin \theta} \simeq \frac{h}{q} \quad (2.2)$$

so that  $\Delta r$  is inversely proportional to the momentum  $q$  transferred to the photons or other particles in an incident beam, when these are scattered by the target. At the beginning of the twentieth century, energies of particle-beam reached only a few MeV, so the resolution was so poor that protons and neutrons could be regarded as elementary and pointlike particles. Nowadays, with a resolution thousands of times better, these are quarks and leptons.

The second reason for high energies is quite simple: many of (predicted) elementary particles are extremely massive, so we need corresponding energy  $E = mc^2$  to

create them. For example, the heaviest elementary particle - the *top* quark - has  $mc^2 \simeq 174$  GeV, nearly 200 times the mass-energy of a proton.

The third reason is connected with attempts to study the matter at extremely high temperature and density, the same conditions as a few microseconds after the *Big Bang*. The aim is generating the *quark-gluon plasma* (*QGP*) - the phase of matter which contains deconfined quarks and gluons (they exist as *free* particles).

## 2.2 Large Hadron Collider

The **L**arge **H**adron **C**ollider (LHC) is being finished<sup>1</sup> at CERN, the world's largest particle physics laboratory, located at the Franco-Swiss border near Geneva. The LHC is a *synchrotron*, a particular type of cyclic particle accelerator which uses electrical field to accelerate particles and variable magnetic field to keep them on a track with constant radius. It is stored in the circular tunnel 26.659 km in circumference which is buried from 50 to 175 m underground. This tunnel was previously occupied by **L**arge **E**lectron-**P**ositron Collider (LEP).

The LHC is an accelerator designed to collide protons with the center-mass-energy of 14 TeV and also heavy ions (like nuclei of lead,  $\text{Pb}^{82+}$ ) with center-mass-energy of 1150 TeV. The beams will be prepared in accelerators chain (see Fig. 2.1) until they reach the energy of 450 GeV and then injected into the LHC.

The Large Hadron Collider has not only the largest energy, it also has very large *luminosity* ( $L$ ) which is defined as

$$N_{events} = L\sigma_{events} \quad (2.3)$$

where  $N_{events}$  is the number of events and  $\sigma_{events}$  is cross the section of studied collision. The LHC aims for luminosity of  $L = 10^{34} \text{ m}^{-2} \cdot \text{s}^{-1}$ . To achieve this value, the beams have to have the corresponding density - in each beam there will be 2808 bunches of  $10^{11}$  particles. Bunches will be separated by 25 ns, thus the bunch crossing rate will be 40 MHz.

The beams will be running in separate pipes in opposite directions. In these pipes there will be an ultrahigh vacuum, the pressure will be  $10^{-13}$  atm (it is about ten times lower than on the Moon). Because of the same charge of each beam, the only way to make the beams run in opposite directions is to have differently

---

<sup>1</sup>May 2008

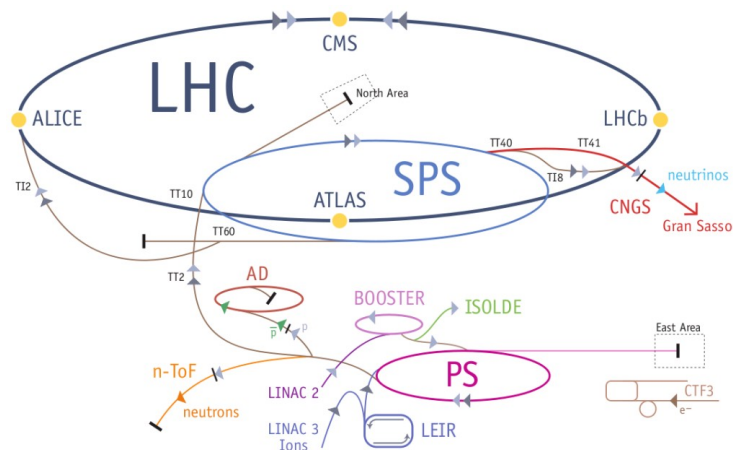


Figure 2.1: Chain of the CERN accelerators. Beams start at the LINAC2 (protons) or LINAC3 (ions) and go through the BOOSTER, Proton Synchrotron and Super Proton Synchrotron into the LHC. Figure from [24].

oriented magnetic field in each pipe. The LHC will use magnets with two sets of coils and two beam channels, because there is not enough place in the LEP tunnel to install two separate rings (see Fig. 2.2 for the LHC tube cross section). The magnets are superconducting and will be cooled to 1.9 K which is lower temperature than in the known universe. The produced magnetic field will be about 8.33 T. The LHC uses two main types of magnets: *dipoles* and *quadrupoles*. 1232 dipole magnets keep the particles on the orbit. Each dipole is 14.3 m long and weights about 35 t. The quadrupoles focus the beam down to the smallest possible size at the collision points. There are 392 quadrupoles.

The LHC is not a perfect circle. It is made of eight arcs and eight *insertions*. The arcs contain the dipole magnets, with 154 in each arc. An insertion consists of a long straight section plus two transition regions. The exact layout of the straight section depends on the specific use of the insertion: physics (beam collisions within an experiment), injection, beam dumping, beam cleaning. The LHC ring is also divided into *octants*. An octant starts from the middle of an arc and ends in the middle of the following arc and thus spans a full insertion. The described scheme and locations of experiments are on the Fig. 2.3.

The LHC is expected to be cooled down at the end of June 2008. At the end of July, first particles may be injected, and the commissioning with beams and collisions will start. In October, first collisions at 10 TeV are expected. The winter shut-down will then be used to commissioning and train the magnets up to full

current, such that the 2009 run will start at the full 14 TeV design energy<sup>2</sup>.

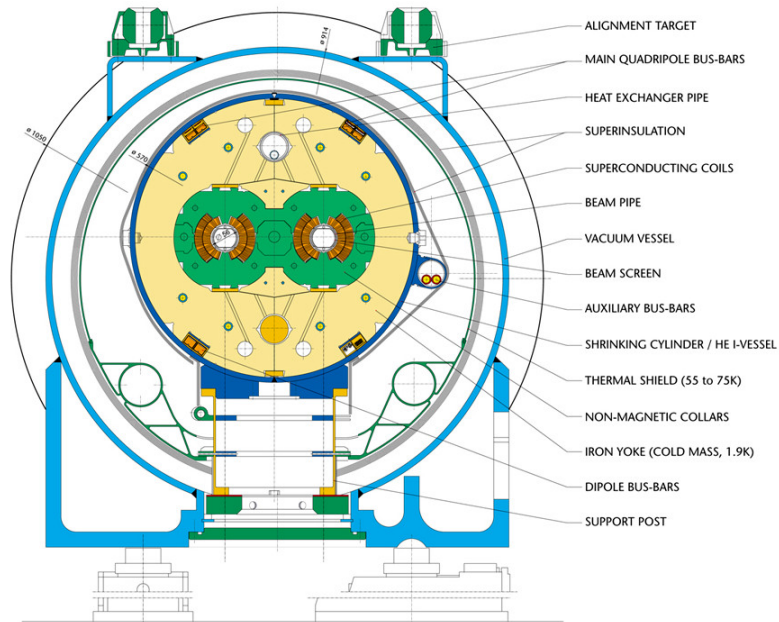


Figure 2.2: Cross section of the LHC tube. Figure from [22].

---

<sup>2</sup>The LHC start-up plans from May 2008

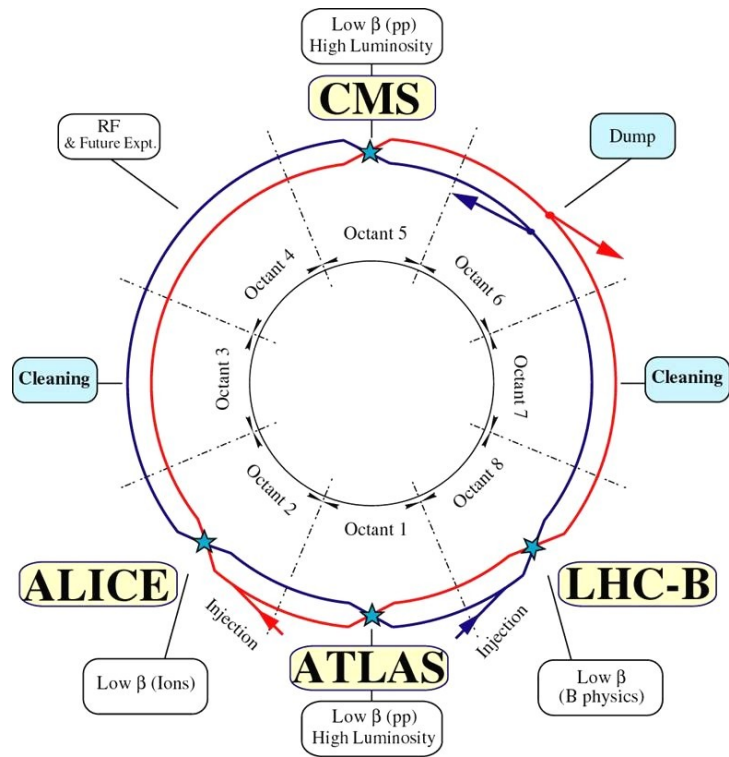


Figure 2.3: The scheme of the LHC and locations of its experiments. Figure from [23].

The main goal of the LHC is to detect the Higgs boson, and thus prove the last part of the Standard Model. It should have also capability to explore the region of energies of the *Beyond the Standard Model* theories (see section 1.2). The LHC will also provide detailed study of the decay of B-mesons (bounded states of  $b$ -quark and some other quark) and thus tell us more about  $CP$ -violation. Last but not least is study of a mentioned  $QGP$ . On the other hand, the LHC may also “create” something absolutely unexpected. That is the reason, why the LHC experiments (described below) should be more universal, not just for “today’s” physics.

To measure the outcome of the LHC, there are six experiments along the course of the accelerator ring:

**ALICE** (**A Large Ion Collider Experiment**) is a detector specialized in analysing heavy ion collisions and it will study the properties of quark-gluon plasma. Nuclei will have an energy of 5.5 TeV per nucleon and their collisions will generate temperatures more than 100 000 times hotter than the heart of the sun. The  $QGP$  will be then identified thanks to the specific signatures of leaving particles.

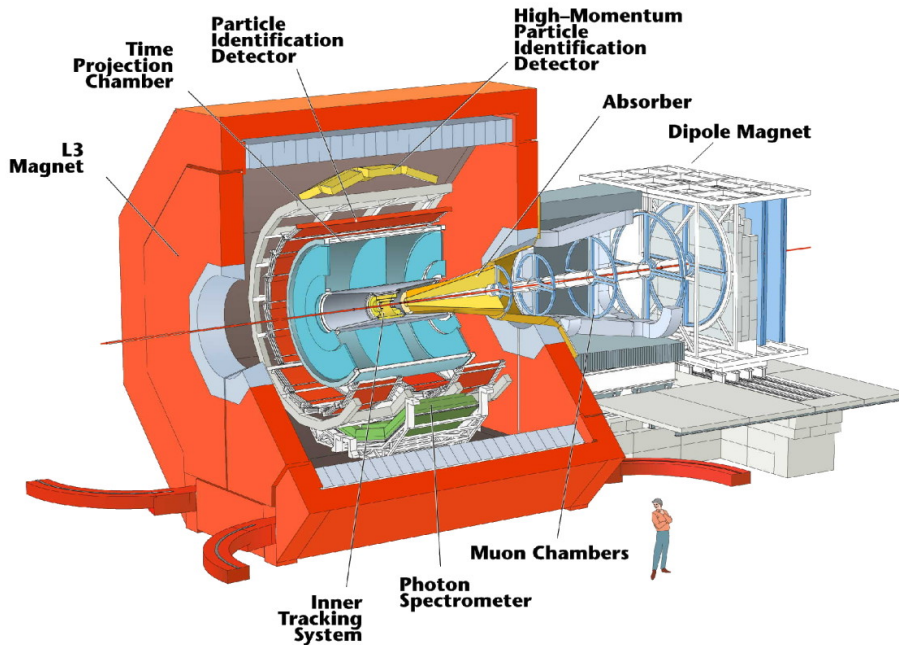


Figure 2.4: Schematic view of the ALICE detector. Figure from [25].

The central part of the ALICE detector measure hadrons, electrons and photons. It is made up of an inner tracking system, a time projection chamber for

momentum measurement, and a particle identification system. All is placed in the large solenoid magnet used perviously in the L3 experiment at LEP. The muon spectrometer is outside of the L3 magnet and is shielded by several metres of material (to absorb most particles other than muons). The spectrometer consists of a dipole magnet to bend the trajectory of the muons and a set of detectors to sample the tracks.

- Size: 26 m long, 16 m high and 16 m wide
- Weight: 10 000 t
- Design: central barrel plus single arm forward muon spectrometer

The schematic view of the ALICE experiment is on the Fig. 2.4.

**ATLAS** (**A Toroidal LHC ApparatuS**) is a general-purpose detector designed to cover the widest possible range of physics at the LHC. The main goals of the ATLAS experiment are the search for the Higgs boson, the study of  $CP$ -violation, the precise measurement of mass of heavy particles, the search for appropriate superparticles or extra dimensions and for particles that could make up *dark matter* - a (still hypothetical) form of matter that does not emit or reflect enough electromagnetic radiation to be observed directly, but whose presence can be inferred from gravitational effects.

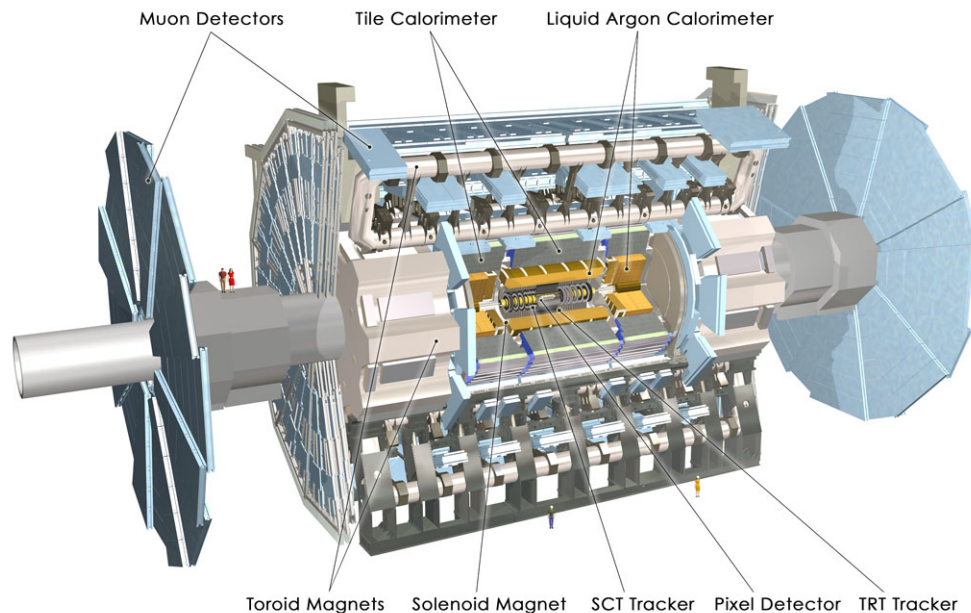


Figure 2.5: Schematic view of the ATLAS detector. Figure from [22].

ATLAS is the largest-volume collider-detector ever constructed. The collaboration consists of more than 1900 members from 164 institutes in 35 countries (April 2007). Its parts will be described in following section (2.3).

- Size: 46 m long, 25 m high and 25 m wide
- Weight: 7 000 t
- Design: barrel plus endcaps

The schematic view of the ATLAS experiment is on the Fig. 2.5.

**LHCb** (**L**arge **H**adron **C**ollider **b**eauty) specializes in the study of the slight asymmetry between matter and antimatter present in interactions of B-particles (particles containing the  $b$ -quark) and thus help us to understand why we live in a Universe that appears to be composed almost entirely of matter, but no antimatter.

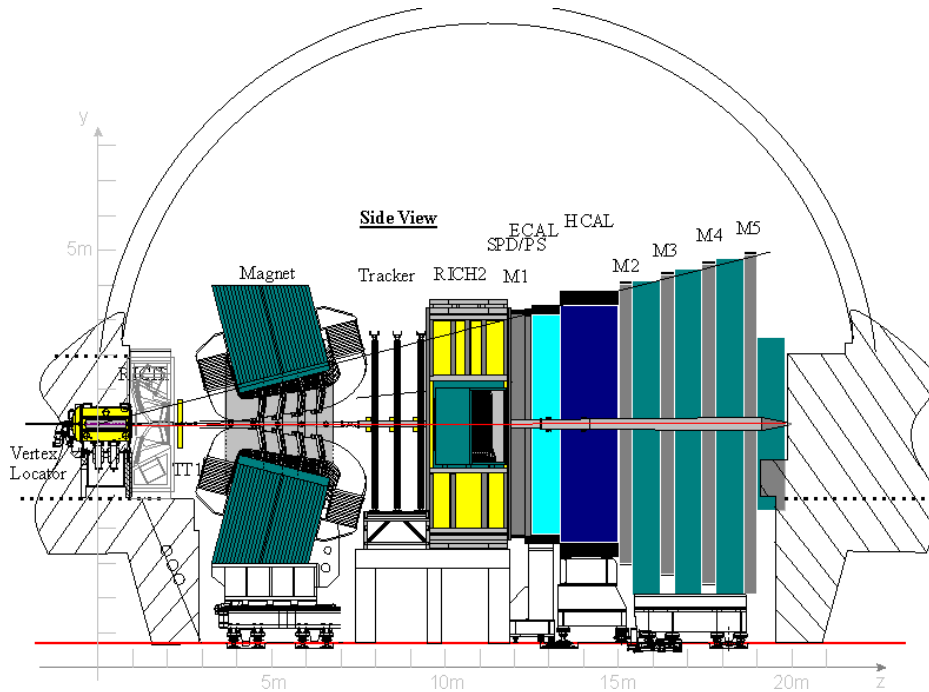


Figure 2.6: Side view of the LHCb detector. Figure from [26].

Instead of surrounding the entire collision point with an enclosed detector, the LHCb experiment uses a series of subdetectors to detect mainly forward particles. The first subdetector is built around the collision point, the next ones stand one behind the other, over a length of 20 m. LHCb is composed by the vertex locator, two RICH (**R**ing **I**maging **C**herenkov) detectors (for

particle identification), the magnet (consists of two coils, both weighing 27 tonnes, mounted inside a 1 450 t steel frame), silicon and outer trackers, electromagnetic and hadron calorimeters and the muon system.

- Size: 21 m long, 10 m high and 13 m wide
- Weight: 5 600 t
- Design: forward spectrometer with planar detectors

The side view of the LHCb experiment is on the Fig. 2.6.

**LHCf** (**L**arge **H**adron **C**ollider **f**orward) is a small experiment designed for astroparticle physics. It will measure particles produced very close to the direction of the beams in the  $pp$  collisions. The motivation is to test models used to estimate the primary energy of the ultra high-energy cosmic rays.

LHCf is composed of two independent detectors for background rejection and redundancy. They are located  $\pm 140$  m from Point 1 (ATLAS).

- Size: two detectors, each measures 30 cm long, 10 cm high and 10 cm wide
- Weight: 40 kg each

**CMS** (**C**ompact **M**uon **S**olenoid) is also a general-purpose detector, optimized for tracking muons, and the word “compact” means that is smaller than the ATLAS detector. CMS and ATLAS have the same physics goals, but different technical solutions and design. That means they can independently confirm the results flowing from the same physical phenomena and reduce systematic and random errors. Moreover, CMS will also try to study heavy ion collisions and the  $QGP$ .

CMS is built around a huge superconducting solenoid which will generate a magnetic field of 4 T. The basic structure of the detector is very similar to ATLAS. The innermost part is the inner tracking system, the next electromagnetic and hadron calorimeters. CMS uses three layers of muon detectors which are placed outside of the superconducting solenoid.

- Size: 21 m long, 15 m high and 15 m wide
- Weight: 12 500 t
- Design: barrel plus endcaps

The schematic view of the CMS experiment is on the Fig. 2.7.

**TOTEM** (**T**OTAL **E**lastic and diffractive cross section **M**easurement) will measure the effective size or “cross-section” of the proton at LHC, study forward

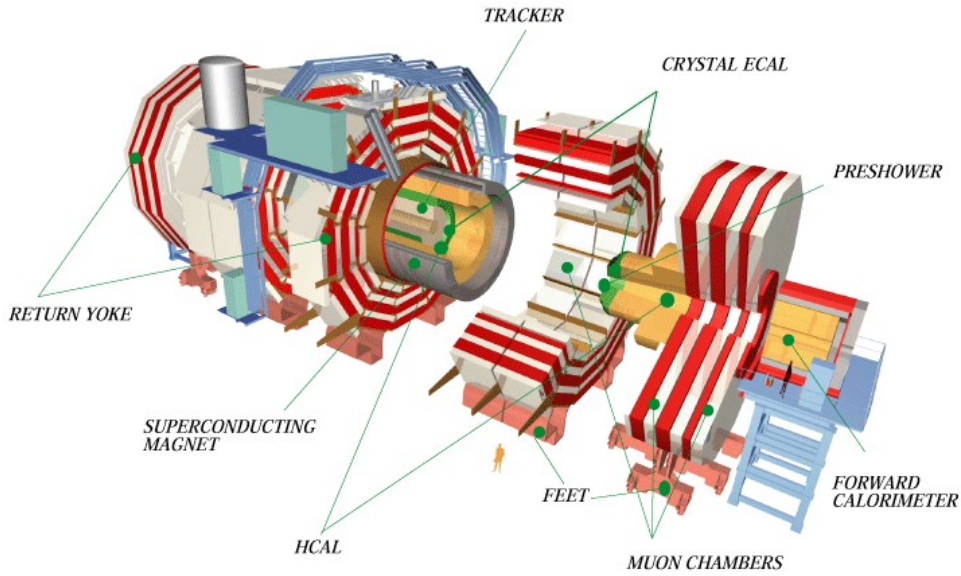


Figure 2.7: Schematic view of the CMS detector. Figure from [26].

particles to focus on physics that is not accessible to the general-purpose experiments and also independently monitor the luminosity of the LHC. To do this it must be able to detect particles produced very close to the LHC beams.

TOTEM will include detectors housed in specially designed vacuum chambers (*Roman pots*) which are connected to the beam pipes. Eight Roman pots will be placed in pairs at four locations near the collision point of the CMS experiment. Although the two experiments are scientifically independent, TOTEM will complement the results obtained by the CMS detector and by the other LHC experiments overall.

- Size: 440 m long, 5 m high and 5 m wide
- Weight: 20 t
- Design: roman pot, GEM detectors and cathode strip chambers

The side view of the TOTEM experiment is on the Fig. 2.8.

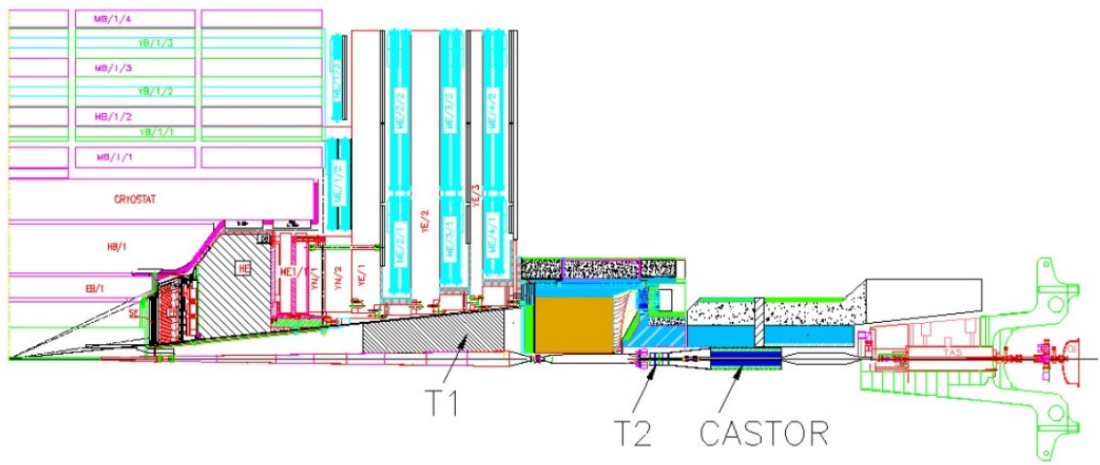


Figure 2.8: Side view of the TOTEM detector. Figure from [20].

## 2.3 The ATLAS Experiment

Because of the ambitious goals, mentioned in the previous section, ATLAS has to be very complex, have high resolution tracking and precise energy measurements. To build up such complicated detector, that was a huge scientific and engineering challenge. However now<sup>3</sup>, with the aid of thousands people, the ATLAS detector is nearly finished.

The ATLAS detector consists of four major components: the *Inner detector* which measures tracks of all charged particles, the *calorimeter* which measures the energies carried by the particles, the *muon spectrometer* which identifies and measures muons and the *magnet system*. The schematic view of the whole detector with all mentioned components is on the Fig. 2.5. A basic scheme of a particle identification in the ATLAS detector is on the Fig. 2.9.

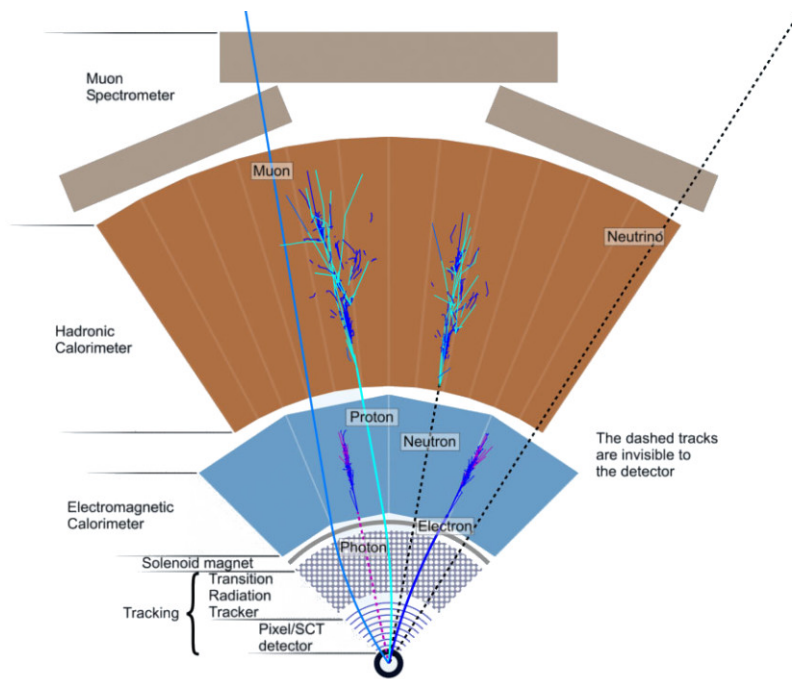


Figure 2.9: A basic scheme of a particle identification. Figure from [22].

---

<sup>3</sup>May 2008

### 2.3.1 Inner Detector

The Inner detector combines high-resolution detectors at the inner radii with continuous tracking elements at the outer radii, all contained in the central solenoid which provides a nominal magnetic field of 2 T. The outer radius is 1.15 m and the total length is 7 m. The Inner detector should give us detailed tracking information about the first part of the particle's trajectory - it covers a pseudorapidity<sup>4</sup> range up to  $|\eta| < 2.5$ . The momentum and vertex resolution requirements from physics call for high-precision measurements to be made with fine-granularity detectors, given the very large track density. Semiconductor tracking detectors, using pixel and silicon microstrip technologies offer these features. As shown on the Fig. 2.10, the Inner detector consists of three subsystems which will be described below.

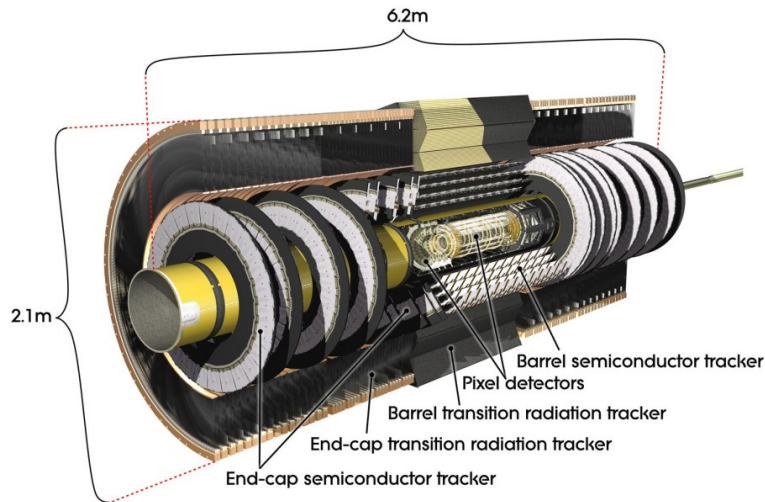


Figure 2.10: Schematic view of the ATLAS Inner detector. Figure from [22].

#### Pixel Detector

The Pixel detector is the innermost part of the Inner detector. It provides a very high-granularity, high-precision set of measurements as close to the interaction point as possible. The system determines the impact parameter resolution and the ability of the Inner detector to find short-lived particles such as  $B$  hadrons and  $\tau$  leptons.

<sup>4</sup>Pseudorapidity is defined as  $\eta = -\ln \tan(\frac{\theta}{2})$  where  $\theta$  is polar angle. Particles flying perpendicular to the beam have zero pseudorapidity and particles flying parallel with beam have infinite pseudorapidity.

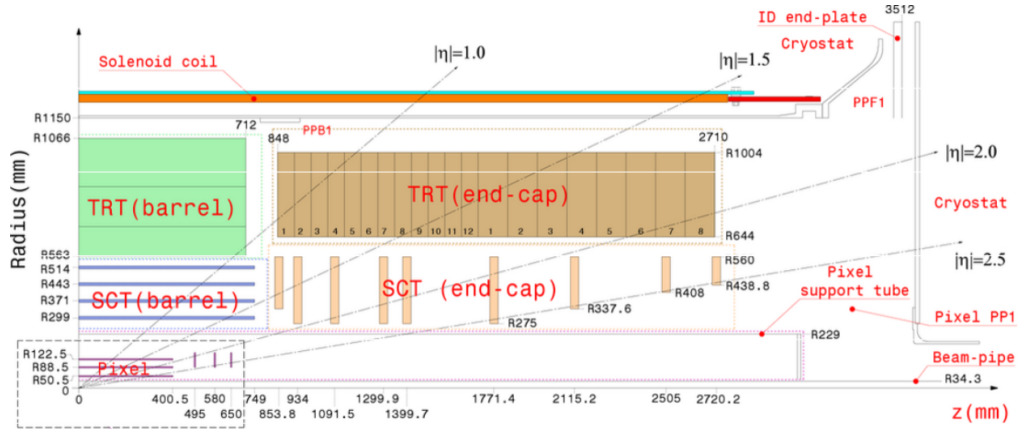


Figure 2.11: Plan view of a quarter-section of the ATLAS Inner detector showing each of the major elements with its active dimensions. Figure from [27].

The detector consists of three barrels and three disks of each endcap. All is shown on the Fig. 2.12. The barrel part of the Pixel detector consists of three cylindrical layers: *B-layer* (with the radius 50.5 mm), *Layer 1* (radius 88.5 mm) and *Layer 2* (radius 122.5 mm). These three barrel layers are made of identical staves inclined with azimuthal angle of  $20^\circ$ . There are 22, 38 and 52 staves in each of these layers respectively. Each staff is composed of 13 pixel modules (or so-called “wafers”). One endcap disk is made of 8 sectors, with 6 modules in each sector. So there are 1744 pixel modules altogether: 288 on the endcap disks and 1456 on the barrel layers (disk modules are identical to the barrel modules, except the connecting cables).

The wafer dimensions are  $16.4 \text{ mm} \times 60.8 \text{ mm}$  and on each there are 16 front-end chips and one module control chip. One front-end chip contains 16 columns of  $400 \mu\text{m}$  and 2 columns of  $600 \mu\text{m}$  (so-called *long*) pixels, and 160 normal plus 4 ganged rows of  $50 \mu\text{m}$  pixels. Thus, the short side of the module has a  $50 \mu\text{m}$  pitch and the long side has a  $400 \mu\text{m}$  pitch with the only exception of long and ganged pixels. The resolution of the pixels is  $14 \mu\text{m} \times 115 \mu\text{m}$ . In total there are 46080 pixels on one module. One pixel module is shown on the Fig. 2.13.

The front-end chips are a major heat source ( $0.8 \text{ W} \cdot \text{cm}^{-2}$ ) dissipating more than 15 kW into the detector volume. This heat is taken out via integrated cooling channels in the detector support elements: staves in the barrel region and sectors in the forward region. Cooling is provided by a  $\text{C}_3\text{F}_8$  evaporative system and keeping sensor temperature stable about  $-10^\circ \text{C}$  during operation.

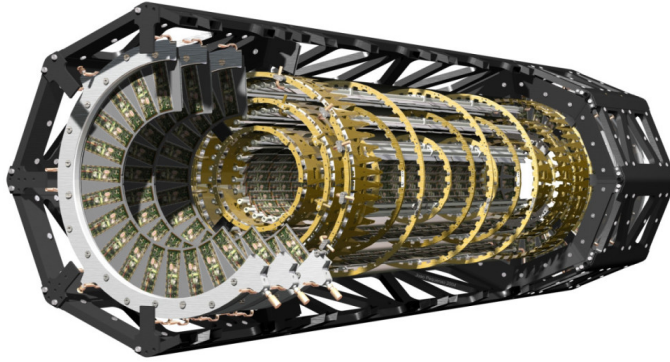


Figure 2.12: 3D model of the Pixel detector. Figure from [22].

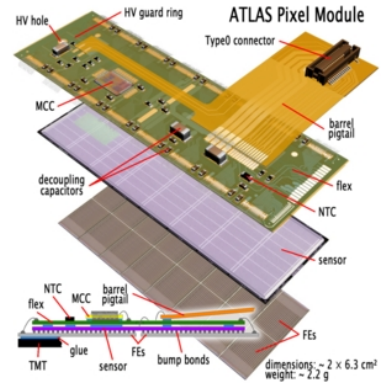


Figure 2.13: The scheme of the single pixel module. Figure from [19].

### Semiconductor Tracker

The second part of the Inner detector is the **SemiConductor Tracker (SCT)**. Its design is very similarly to the Pixel detector, but instead of pixels it uses the silicon strips for detection. This system will provide eight precision measurements per track in the intermediate radial range, contributing to the measurement of momentum, impact parameter and vertex position.

The barrel part of the detector uses eight layers of silicon microstrip detectors to provide precision position measurement. The modules are mounted on carbon-fibre cylinders which carry the cooling system. The barrels have radius of 30.0 cm, 37.3 cm, 44.7 cm and 52.0 cm respectively. The endcap modules are mounted in up to three rings onto nine wheels, which are interconnected by a space-frame. Each silicon detector is 6.36 cm × 6.40 cm with 768 readout strips of 80 μm pitch.

### Transition Radiation Tracker

The last part of the Inner detector is the **Transition Radiation Tracker (TRT)**. It is based on the use of straw detectors, which can operate at the expected high rates due to their small diameter. This system detects the transition radiation photons which were created by passing particles.

The barrel contains about 50 000 straws, each divided in two at the center, and the endcaps contain 320 000 radial straws. Each straw is 4 mm in diameter and

equipped with a  $30\ \mu\text{m}$  diameter gold-plated wire. The maximum straw length is 144 cm in the barrel, in the endcap they are a bit smaller. Because of a large number of the straws, TRT produces about 35 hits for each track.

### 2.3.2 Calorimeters

The calorimeter measures the energies of charged and neutral particles. In general, it is made of metal sheets and a detection medium. Whenever a particle meets the absorber, it interacts with the material and produces a shower of secondary particles which are detected in the detection medium. ATLAS has two types of calorimeters (see Fig. 2.14 for the scheme of the calorimeter system):

#### Electromagnetic Calorimeter

In the EM calorimeter, the absorbers are made of lead and the detection medium is liquid argon (*LAr*). The space filled with liquid argon is under an intense electric field (2000 V over 2 mm). Particles in the shower produce ionization electrons which drift through the *LAr*. This electrical current is then detected on copper electrodes and the energy of the original electron can be calculated from its value.

The EM calorimeter is divided into a barrel part and two end-caps. The barrel calorimeter consists of two identical half-barrels, separated by a small gap (6 mm) at  $z = 0$ . Each end-cap calorimeter is mechanically divided into two coaxial wheels.

#### Hadron Calorimeter

The hadronic calorimeter surrounds the electromagnetic calorimeter. It measures the energies of hadrons ( $p$ ,  $n$ ,  $\pi$ ,  $K$  and other), electrons and photons have been stopped before reaching it (see Fig. 2.9 for the scheme of the ATLAS particle identification). The hadronic calorimeter makes use of steel as the absorber material and scintillating plates read out by wavelength shifting (*WLS*) fibres as the active medium. Interactions of high energy hadrons in the plates transform the incident energy into a “hadronic shower” which traversing through the scintillating tiles causes them to emit light which is then measured.

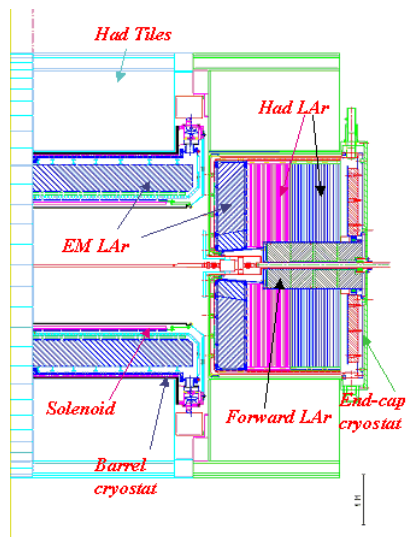


Figure 2.14: The scheme of the ATLAS calorimeters. Figure from [22].

### 2.3.3 Muon Spectrometer

The only charged particle that can travel through all of the calorimeter material are muons. They lose energy almost entirely by the formation of electron-ion pairs along their path, and for a substance like steel, this amounts to an energy loss of about 1 MeV per millimeter of path. Thus muons with energy above 5 GeV will penetrate about 5 m of steel, whereas hadrons of almost any energy are completely absorbed in about 1.5 m of steel. Thus energetic particles seen outside the hadron calorimeter are guaranteed to be muons.

The Muon System determines the signs and momenta of muons with better precision than the inner tracking system does. In the barrel region ( $|\eta| < 1$ ), muons are measured in three layers of chambers consisting of precise *Monitored Drift Tubes* (*MDTs*) and fast *Resistive Plate Chambers* (*RPCs*) used for triggering. In the endcap regions, also three layers of chambers are installed, but vertically. Here *Thin Gap Chambers* (*TGCs*) are used for triggering. The precision measurement of muons is again done with *MDTs*, except for the innermost ring of the inner station of the end caps and for  $|\eta| > 2$ , where high particle fluxes require the more radiation tolerant *Cathode Strip Chamber* (*CSC*) technology.

### 2.3.4 Magnet System

To bend the tracks of charged particles, ALTAS uses two systems of magnets. The first is solenoid between the Inner Detector and the calorimeters. It has a length of 5.3 m with a bore of 2.4 m and it is designed to provide a field of 2 T with a peak magnetic field of 2.6 T.

The second system consists of eight Barrel coils housed in separate cryostats and two endcap cryostats housing eight coils each. The endcap coils systems are rotated by  $22.5^\circ$  with respect to the Barrel Toroids in order to provide radial overlap. The Barrel coils have an axial length of 25.3 m and extend radially from 9.4 m to 20.1 m. They provide the peak field of 3.9 T. The endcap coils have an axial length of 5 m and extend radially from 1.65 m to 10.7 m. The peak field provided by them is 4.1 T.



# Chapter 3

## ATLAS Computing

The ATLAS detector will produce huge amount of data: in the LHC, under nominal operating conditions, each proton beam has 2808 bunches, with each bunch containing about  $10^{11}$  protons. The bunch spacing is 25 ns which gives us a peak crossing rate of 40 MHz. However, for practical reasons there are several bigger gaps in the pattern of bunches, which allow time for example for the “kicker” magnets to come on in order to inject or dump beam. The average crossing rate is equal to the total number of bunches multiplied by the number of turns round the LHC per second:  $2808 \times 11245 = 31.6$  MHz. Times approx. 20  $pp$  collisions per crossing at nominal luminosity gives more than  $6 \times 10^8$  inelastic events per second. It is impossible to store and analyze that amount of data and moreover, not every collision will be interesting. For these reasons, ATLAS uses a system of triggers and various data formats.

### 3.1 ATLAS Trigger

The main task of the ATLAS trigger is not easy: it has to reduce a flux of information from  $10^9$  Hz to 200 Hz, but it must not to discard interesting events (for example, a Standard Model Higgs particle with a mass of 120 MeV, decaying into two photons, is expected to occur at a rate of  $10^{-13}$  of the interaction rate... the proverbial pin in the haystack).

The triggering process is divided into three steps. The first step (L1 trigger) is implemented as a hardware trigger, the second and third steps (L2 trigger and

Event Filter) are software triggers and are usually referred to as the ATLAS High Level Trigger (HLT). The scheme of the ATLAS trigger is shown on the Fig. 3.1.

L1 trigger reduces the initial 40 MHz to less than 75 kHz in less than 2.5  $\mu$ s. It looks for regions of potentially interesting activity in the Calorimeters and the Muon Spectrometer that may correspond to candidates for high  $p_T$  leptons, hadrons or jets. This is known as Region of Interest (ROI) concept (see Fig. 3.2).

The L2 trigger selection uses the ROI information of the L1 trigger for its processing. This strategy keeps the amount of raw data to be passed for processing at only a few percent of the full event information: the L2 trigger reduces the rate to approx. 1 kHz and its latency is about 10 ms.

Event Filter further reduces the rate to frequency of about 200 Hz (latency is approx. 1 s). The raw data of the full event are passed to the Event Builder, which collects the pieces of information connected to this event and put them into a single memory. The size of each event saved at the permanent data storage is about 1 MB.

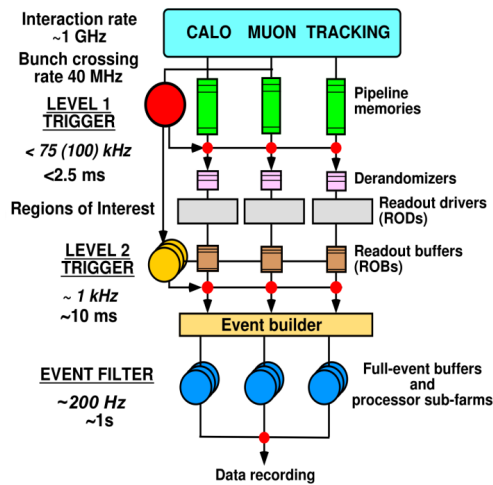


Figure 3.1: The scheme of the ATLAS trigger. Figure from [21]

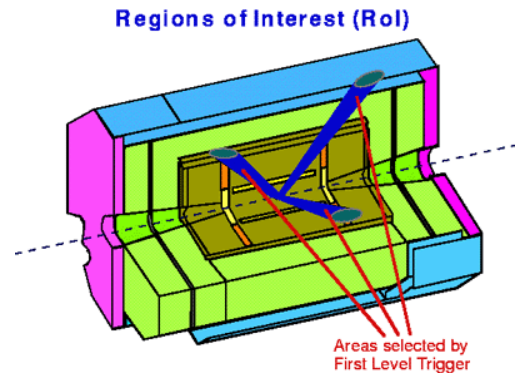


Figure 3.2: An example of Regions of interest selected by L1 trigger. These are used by the further trigger levels. Figure from [22]

## 3.2 ATLAS Offline Software

Every physicist has own ideas and thus special needs in a data analysis. That means there cannot be just one programme. On the other hand, it is rather ineffective to

write a whole algorithm, apart from the fact that not every physicist is such a good programmer. The solution is a software framework, which contains a set of common methods and data types which are then used to construct more complex algorithms. In the case of the ATLAS experiment, that framework is called **Athena**.

The Athena framework is based on C++ and is an enhanced version of the Gaudi framework that was originally developed by the LHCb experiment, but is now a common ATLAS–LHCb project. Athena and Gaudi are concrete realizations of a component-based architecture (also called Gaudi) which was designed for a wide range of physics data-processing applications.

Athena uses a unified hierarchy of data types. Each of them has some advantages and disadvantages (mainly the size):

**RAW data** data are events as output by the Event Filter (see section 3.1) for reconstruction. The event size should be about 1.6 MB, arriving at an output rate of 200 Hz.

**ESD (Event Summary Data)** refers to event data written as the output of the reconstruction process. Its content is intended to make access to RAW data unnecessary for most physics applications other than for some calibration or re-reconstruction. ESD has an object-oriented representation, and is stored in POOL ROOT files. The size of an event is about 500 kB

**AOD (Analysis Object Data)** is a reduced event representation, derived from ESD, suitable for analysis. It contains physics objects and other elements of analysis interest. As ESD, AOD has also an object-oriented representation, and is stored in POOL ROOT files. The target size is 100 kB per event.

**TAG data** are event-level metadata - thumbnail information about events to support efficient identification and selection of events of interest to a given analysis. The assumed average size is 1 kB per event.

**DPD (Derived Physics Data)** is an n-tuple-style representation of event data for end-user analysis and histogramming.

**SIM (SIMulated Event Data)** refers to a lot of data types, beginning with generator events through simulation of interactions with the detector and of detector response. The storage technology is POOL ROOT files. SIM are often larger than RAW (approx. 2 MB in size), in part because they usually retain Monte Carlo “truth” information.

Athena is not only the reconstruction and analysis algorithms for the ATLAS data, but it contains also all other software needed for the HEP computing. All these software together form a software chain which is needed to produce the AOD file on which analysis can be performed. The diagram of this *Full Software Chain* is shown on the Fig. 3.3.

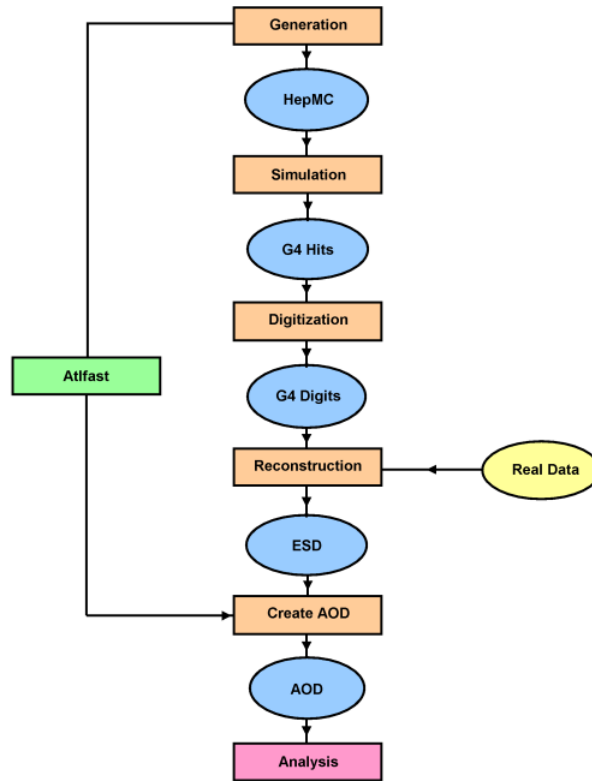


Figure 3.3: The Athena full software chain diagram. Figure from [28].

**Generation** Generators create an output of some physical process. If we know the initial conditions, we get a list of outgoing particles, their position and momenta. For this job, they employ some Monte Carlo (MC) generator which produces events with the theoretically predicted probability. So the quality of generator is highly dependent on our knowledge of the underlying physics. Generators are crucial in designing the detector, because they tell us what we should expect. Athena includes many generators, typical examples are Pythia and Herwig (both are written in FORTRAN, not in C++).

**Simulation** A simulator takes a Lorentz 4-vector of a particle (created by generator) and the detector geometry and composition. As an output we get

a collection of hits, which may carry information like position, energy deposit, identifier of the active element etc. In Athena there are two types of simulation programmes:

**G4ATLAS** is based on the Geant4 simulation package, which provides both a framework and the necessary functionality for running detector simulation. The functionalities provided include optimized solutions for geometry description and navigation through the geometry, the propagation of particles through detectors, the description of materials, the modelling of physics processes and many more.

**Atlfast** is a fast simulation programme, which replaces the full detector simulation and reconstruction phases of the reconstruction chain (as shown by the diagram on the Fig. 3.3). Fast simulation is performed by smearing the MC truth information directly with resolutions measured in full simulation studies. Atlfast speed depends on many factors, but in general it is 4 or 5 orders of magnitude faster than running the full chain.

**Digitization** In this step, the software takes the hits from simulation and turns them into *what-we-get-from-real-detector*. The algorithm has to take into the account the response of the readout electronics and the imperfection of the detectors like finite resolution, noise or defects. The output files of the digitisation step are called Raw Data Objects (RDOs) and should resemble the real data from the detector. This has at least two advantages: RDOs can be used for preparing of our computers for what they can see in the real experiment and also, we can compare the digitized data with real data and thus test the quality of our generators and simulators.

**Reconstruction** The main task of the reconstruction is to derive from the stored RAW data the relatively few particle parameters and auxiliary information necessary for physics analysis. That means to find hits, try to fit a track through them and save it together with vertices, jets, missing energy etc. Information from all detectors is combined - common tools are shared between tracking detectors on one side (Inner Detector and muon chambers - see sections 2.3.1 and 2.3.3) and calorimeters (see 2.3.2) on the other side. The output is stored in ESD and AOD formats (see above).

**Analysis** In this phase, we have real or simulated data in AOD files and now we need physicists with their intuition. They should interpret the reconstruction results and try to find what actually happened. For this purpose, every physicist can write his analysis algorithm and then visualize the results in some software - pictures are more comprehensible for human mind than numbers. There are two ways to do this:

The first one is to plot a histogram. The most used programme is **ROOT**, which is very popular in HEP community. It is an object-oriented framework and is also written in C++. Both frameworks, ROOT and Athena, are well connected. ROOT can be used in an interactive mode (writing the C++ statements on the CINT command line) or it is possible to write a script and then execute it. It is very powerful and universal software, which can be use for example for histogramming and graphing to visualize and analyze distributions and functions, curve fitting (regression analysis) and minimization of functionals, statistics and data analysis, matrix algebra, but also for drawing the Feynman diagrams or 3D visualization of the detector.

The second way is to use an event viewer. In the case of ATLAS, the viewer is called **Atlantis**. It is a stand-alone Java application, which uses simplified detector geometry. Atlantis can be used for the visual investigation and the understanding of the physics of complete events. It is also a tool for creating pictures and animations for publications, presentations and exhibitions. JiveXML (event converter) is C++ interface between Atlantis and the Athena framework.

# Chapter 4

## Testing ATLAS Pixel Detector With Cosmic Muons

In section 2.3, the ATLAS detector was described in detail. It would be unwise to put together so complicated detector without previous testing of its components. In the case of the ATLAS Pixel Detector (see 2.3.1) there are at least two ways how to do that. The first way is so-called test beam (produced by some accelerator). These test beams were performed, for example, at the CERN SPS using a pion beam of 180 GeV/c momentum. The second way is to use cosmic rays. Cosmic rays were used as a source of new particles during first years of HEP and thus intensively studied. Now we know cosmic rays so well that we can use them for calibration and commissioning of our experiments.

### 4.1 Cosmic Muons

Every second the Earth's atmosphere is bombarded with high-energy particles coming from all directions from outer space. They are produced in events such as supernovas or the formation of black holes, during which they can be accelerated to enormous energies. The observed energy spectrum is very wide, ranging from  $10^9$  eV to over  $10^{20}$  eV. This spectrum is shown on the Fig. 4.1.

Almost 90 % of all the incoming cosmic rays are protons, about 9 % are alpha particles and about 1 % are electrons. The remaining fraction is made up of the other heavier nuclei (with an atomic number between 2 and 92). Incoming particles collide with molecules of air in the Earth atmosphere. In this process

mostly pions and kaons are created and they further decay to photons, electrons, muons and neutrinos. This *cosmic ray shower* also contains a hadronic core, which can interact with molecules of air again. An example of this shower is shown on the Fig. 4.2.

We are interested in cosmic muons, because they are the most numerous charged particles at sea level. They are produced typically about 15 km above the ground and lose about 2 GeV to ionization before reaching it. The mean energy of muons at the ground is approx. 4 GeV. Their distribution is  $\propto \cos^2 \theta$  of the incidence angle and is symmetric in  $\varphi$ . The integral intensity of vertical muons above 1 GeV/c at sea level is approx.  $70 \text{ m}^{-2} \cdot \text{s}^{-1} \cdot \text{sr}^{-1}$ , which is frequently presented in the form  $I \approx 1 \text{ cm}^{-2} \cdot \text{min}^{-1}$  for horizontal detectors.

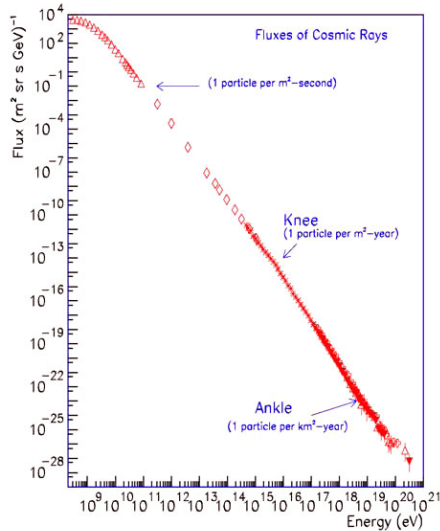


Figure 4.1: The energy spectrum for cosmic rays. The flux of cosmic rays appears to follow a single power law  $\sim E^{-3}$  over the range from  $10^9$  eV to  $10^{20}$  eV. Figure from [37].

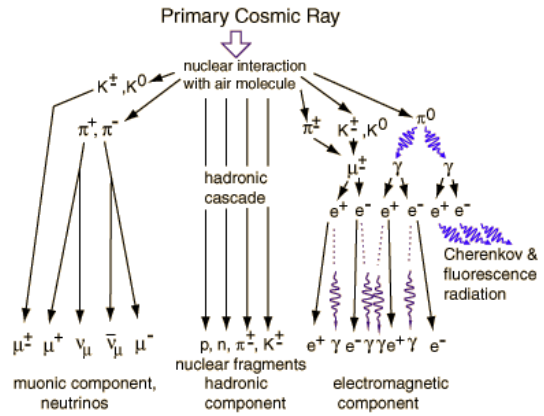


Figure 4.2: A diagram of a cosmic ray shower. It contains hadronic, electromagnetic and muon components (with neutrinos). Figure from [36].

## 4.2 Pixel EndCap Cosmic Test Setup

For this thesis I have chosen the cosmic test of the Pixel EndCap A, which is one of the two end-sections of the pixel part of the Inner detector (see section 2.3.1).

As the other parts of the Pixel detector, also the Pixel EndCap was tested in the surface building *SR1* located at CERN Meyrin Site near Point 1.

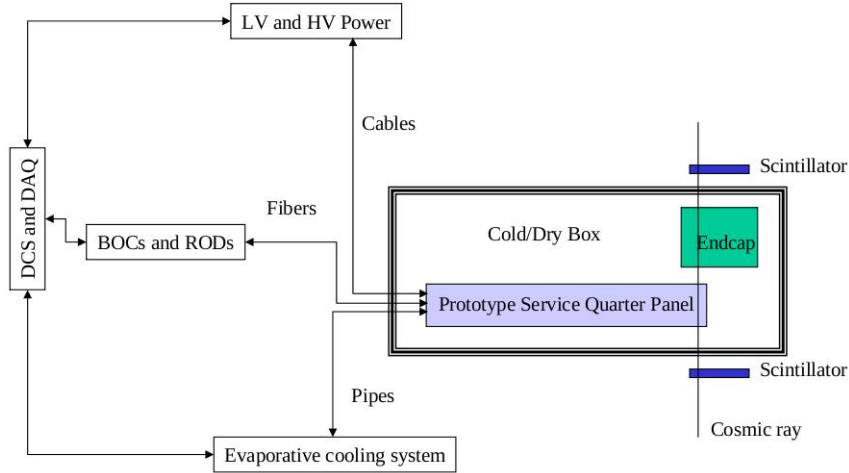


Figure 4.3: The scheme of the Pixel EndCap cosmic test setup. The detector is connected to the PSQP. Both the Pixel EndCap and PSQP are placed inside the dry box, which provide the required environment for the pixel operation. The PSQP is connected to all outside services (cooling, LV and HV distribution and regulation, readout etc.). Figure from [29].

The Pixel EndCap consists of three disks, 48 modules each, which correspond to 8% of the full detector size. The detector is connected to a *Prototype Service Quarter Panel (PSQP)*, which is used to perform the conversion of data signal from electrical to optical and is connected to all outside services (cooling, LV and HV distribution and regulation, readout etc.). Both the Pixel EndCap and *PSQP* are placed inside the dry box (as shown on the Fig. 4.3).

The EndCap hangs vertically inside the dry box, that is an obvious requirement to maximize the flux of cosmic muons passing through it. As is shown on the Fig. 4.4, there is also an iron shielding used to remove low momentum cosmic muons. Total of 20 cm of iron provides a 230 MeV/c momentum cut. 10 cm of iron is on the table ( $\sim 330$  kg) and 10 cm is under the table ( $\sim 680$  kg).

For triggering, four scintillators were placed above and under the Pixel EndCap. Their locations and dimensions are also shown on the Fig. 4.4. The event is recorded if the top scintillator and at least one of the bottom scintillators are hit.

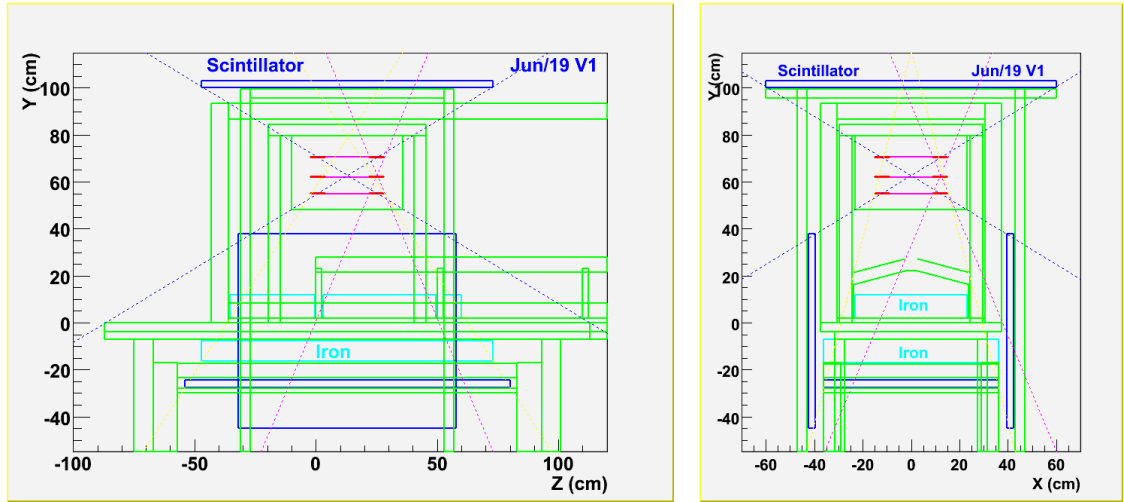


Figure 4.4: Side-view (left) and z-view (right) of the Pixel EndCap A cosmics setup. There are four scintillator planes (in blue) and two iron shieldings (in cyan). Pixel layers are represented by red color. Figure from [29].

### 4.3 Cosmic Data Simulation

The main goal of the simulation chain is to validate the simulation/reconstruction chain from the beginning to the end, i.e. from simulation, digitization, bytestream converter all the way to reconstructed tracks and alignment. The ATHENA release 12.0.0 was used. The full Cosmic Data Simulation is done in the following steps:

**Cosmic muon generator:** cosmic muons were randomly generated by the *CosmicGenerator* package [31] according to all distributions described in [2]. The core of the package is an old Fortran cosmic muon generator, which is based on fits to experimental data from ALEPH. This generator is wrapped up inside the C++ code to provide the necessary interface with other ATHENA packages.

**Pixel EndCap A geometry:** this geometry is identical to the one implemented in *PixelGeoModel* [32]. The only difference is that EndCap C, the barrel of the Pixel detector, support tube, frame and services are switched off. Thus only Pixel EndCap A remains.

**Geant4 detector simulation:** the Geant4 (G4) is described mainly in *G4AtlasApps* package [33]. It contains definition of all setup positions and dimensions: Pixel EndCap A position, scintillator and iron positions and dimensions etc.

**Trigger system simulation:** the scintillators (see section 4.2) are placed in the right position in *G4AtlasApps*. When the cosmic muon passes through them, the energy is deposited in their volume and if it is above some minimum amount it is considered to be a hit in the scintillator system. The logic coincidence between two scintillators is implemented in *InDetCosmicSimAlgs* package [34]. Events without coincidence between the top and at least one of the bottom scintillators are skipped, only triggerable events are passed further to digitization.

**Digitization:** the digitization code makes use of the map of bad pixels (observed during module production) and the list of disable modules to skip simulated hits in inefficient regions.

A detailed and comprehensible Cosmic Data simulation recipe can be found at ATLAS Twiki pages [30].

## 4.4 Real and Simulated Data Comparison

For a comparison between real and simulated data I chose a high statistics run 1129. The first thing I was interested in was the electronic noise. When a cosmic muon fired the trigger, the data were recorded for 16 consecutive BCID (**B**unch **C**rossing **I**D). One BCID is equal to the time between two bunch crossings at full LHC luminosity (thus one BCID lasts 25 ns). Each hit contains the information in which BCID it was collected. Hits with  $BCID = 5$  belong to cosmic muons. This provides a distinction between the random noise (which can have any BCID) and the cosmic signal. A cut of  $|BCID - 5| < 2$  was used for cosmic signals. Pixel hits outside this range were classified as noise hits.

The BCID of all selected (good) pixels is shown on the Fig. 4.5 (bottom). You can see the cosmic peak corresponding to  $BCID = 5$ . A corresponding cluster size (i.e. the number of pixel hits) is on the Fig. 4.5 (top). Apparently in most cases two pixels were hit. On the Fig. 4.6 you can see a comparison of accepted hits and deposited charge in terms of ToT (**T**ime **o**ver **T**hreshold - it tells how long has been a pixel excited to the conductive band by a hit) for normal and ganged pixels. The last (Fig. 4.7) is comparison of the ToT distribution for single, double and triple clusters (for each individual pixel hit and also for total ToT of a cluster).

The second subject of my concern is a cosmic tracking. The tracking algorithm, used by ATLAS Pixel Group, loops over any pair of the pixel clusters from the inner

and outer disks and linearly extrapolates to the middle disk. For any pixel cluster a correspondent cosmic track candidate is reconstructed including a possible hit in the overlap region from the neighboring module. If there are multiple track candidates, the best one is selected based on the number of pixel hits and the fitted chisq ( $\chi^2 < 25/\text{ndof}$ ) in the  $x - z$  and  $y - z$  plane.

On the Fig. 4.8 you can see spherical coordinates ( $\varphi$  and  $\theta$ ) of reconstructed cosmic tracks. Take notice of the influence of triggers location on  $\varphi$  distribution of tracks. Total  $\chi^2$  of the fits and the track probability distribution are shown on the Fig. 4.9 and Fig. 4.10 respectively.

As we can see on all these histograms, the agreements between real cosmic data and Monte Carlo simulations are excellent. It means several things: firstly it is obvious that we have good knowledge of cosmic muons and thus we can simulate them precisely. However, much more important is the fact that the Pixel detector (or at least its EndCap part) and the ATLAS software are well prepared to real data taking.

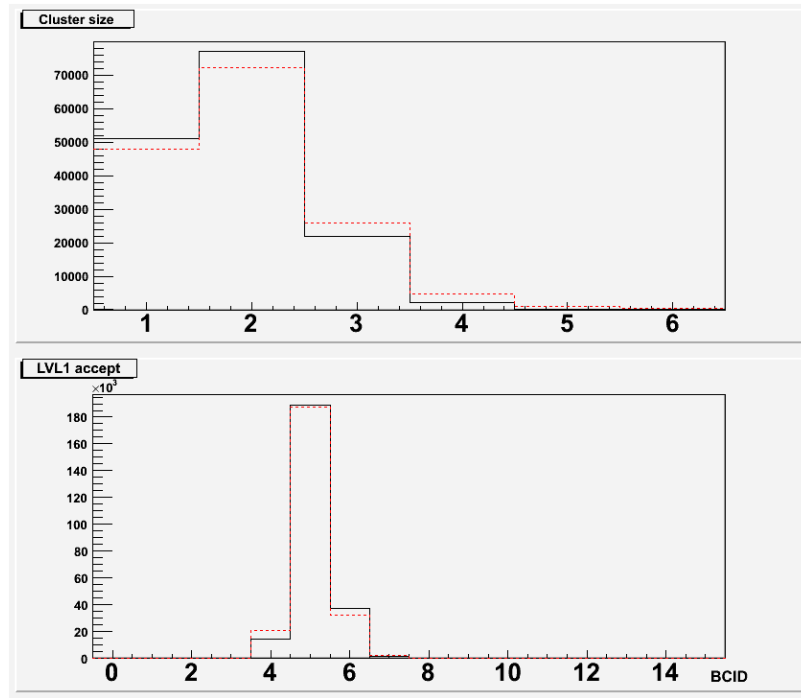


Figure 4.5: Comparison of the cluster size (top) and its BCID (bottom) between real data (black solid line) and Monte Carlo simulation (red dashed line). On the bottom histogram, you can see the cosmic peak corresponding to BCID = 5.

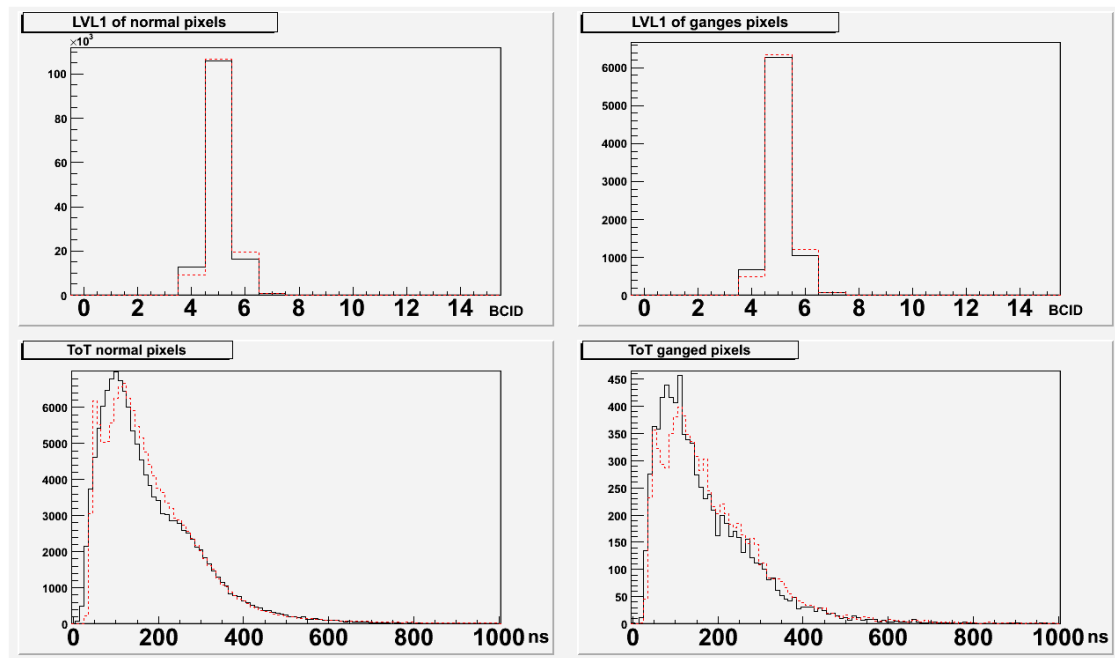


Figure 4.6: Comparison of accepted hits (top) and deposited charge in terms of ToT (bottom) between real data (black solid line) and Monte Carlo simulation (red dashed line). On the left are histograms for normal pixels and on the right are histograms for ganged pixels. You can see peaks about 125 ns. That corresponds with  $BCID = 5$  (cosmic muons).

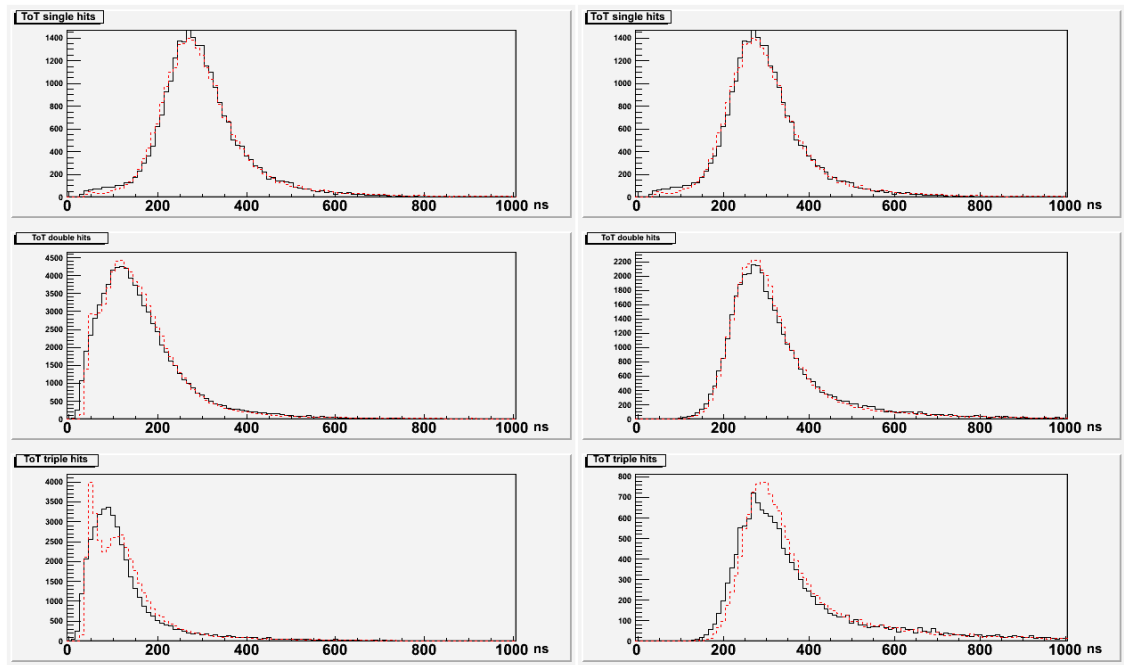


Figure 4.7: Comparison of the ToT distribution for single, double and triple clusters between real data (black solid line) and Monte Carlo simulation (red dashed line) for each individual pixel hit (left) and for total ToT of a cluster (right).

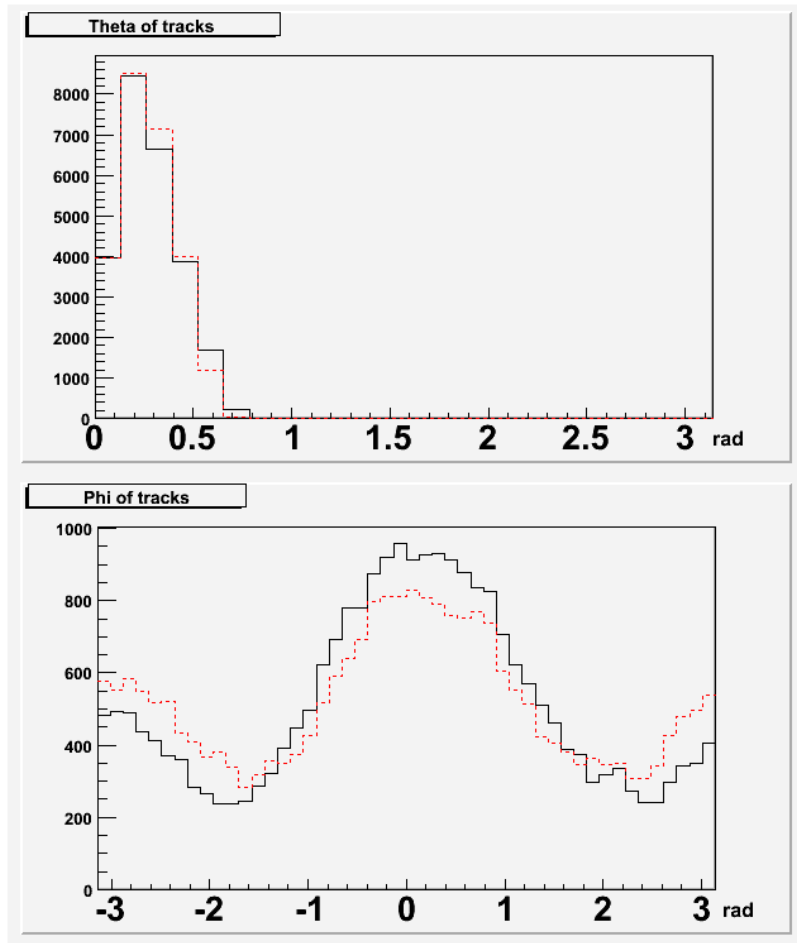


Figure 4.8: Comparisons of the  $\varphi$  and  $\theta$  of the reconstructed cosmic tracks between real data (black solid line) and Monte Carlo simulation (red dashed line). Take notice of the influence of triggers location on  $\varphi$  distribution of tracks.

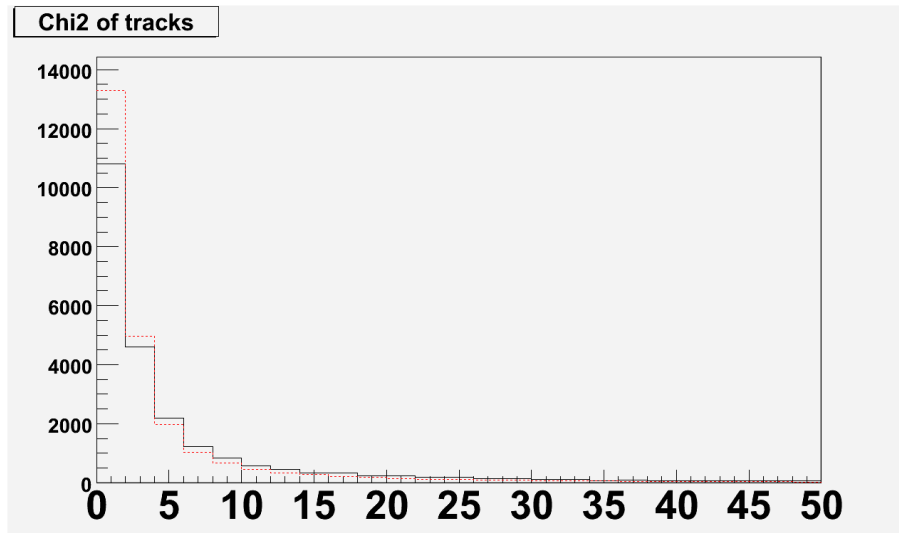


Figure 4.9: Comparisons of cosmic tracking in terms of the  $\chi^2$  of fit between real data (black solid line) and Monte Carlo simulation (red dashed line).

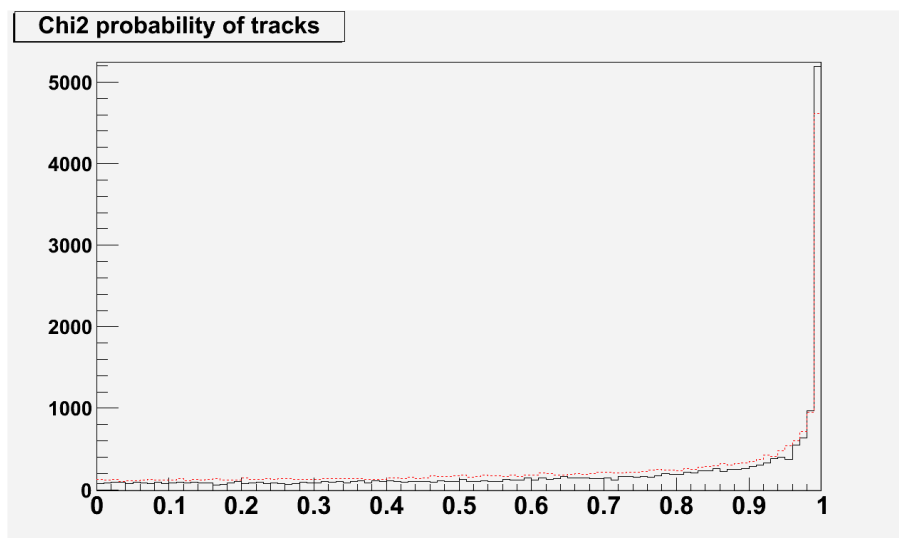


Figure 4.10: Comparison of track probability distribution between real data (black solid line) and Monte Carlo simulation (red dashed line).

# Chapter 5

## Thesis Summary

The first chapter of this thesis presents the basics of the Standard Model, which is still our best describing theory of particles and their interactions. It was formulated in the 1970s and since that time it passed all experimental tests. However, not all of its predictions are already confirmed. A typical example is the Higgs particle which could explain why the carriers of the electroweak force (the  $W$  and  $Z$  bosons) have mass. At the end of the first chapter, some problems beyond the Standard Model are mentioned. This chapter should offer some theoretical knowledge for further chapters.

The second chapter is devoted to high energy physics experiments, mainly to the CERN's flagship project, the Large Hadron Collider (LHC). In this accelerator, protons will collide with energies about 14 TeV. Around the LHC interaction points there are six experiments, whose main purpose is to answer some questions presented in the chapter one. In the second part of this chapter, the largest of mentioned experiments, the ATLAS experiment, is described in detail. This description mainly concerns about the Inner detector.

Because the ATLAS detector will produce huge amount of data (on the LHC there will be more than  $6 \times 10^8$  inelastic events per second), a great computing power will be needed. Some details are presented in the third chapter, called ATLAS Computing. The attention is mainly paid to the ATLAS trigger system and Offline software.

The last chapter is concerned with using cosmic muons for the ATLAS Pixel detector testing. At first the nature of cosmic rays is described. Next part contains the setup of the testing of the Pixel EndCap A in the SR1 building at CERN and

a brief description of the cosmic data simulation. In the end a comparison between real cosmic data and the Monte Carlo simulation is shown. For this comparison I chose a high statistics run 1129. I was interested especially in the electronic noise and in the cosmic tracking. As you can see on all presented histograms, the agreements between real and simulated data are excellent.

This research shows that (at least) the Pixel EndCap A and the ATLAS software are well prepared to real data taking. For me it was also a good practical exercise in using the HEP software, which I will need for my further work.

# Bibliography

- [1] D. H. Perkins, *Introduction to High Energy Physics*, Cambridge University Press, UK, 2000
- [2] W. - M. Yao *et al.* (Particle Data Group), *J. Phys. G* 33, 1 (2006) and 2007 partial update for the 2008 edition available on the PDG web pages: <http://pdg.lbl.gov/>
- [3] T. Morii, C. S. Lim, S. N. Mukherjee, *The Physics of the Standard Model and Beyond*, World Scientific, 2004
- [4] Fayyazudin, Riazuddin, *A Modern Introduction to Particle Physics*, World Scientific, Singapore, 2000
- [5] J. R. Christman, *SU(3) and the Quark Model*, project PHYSNET, MISN-0-282, <http://www.physnet.org>
- [6] P. Langacker, *Structure of the Standard Model*, hep-ph/0304186
- [7] D. Griffiths, *Introduction to Elementary Particles*, John Wiley & Sons, Inc., USA, 1987
- [8] W. N. Cottingham, D. A. Greenwood, *An Introduction to the Standard Model of Particle Physics*, Cambridge University Press, USA, 2007
- [9] M. E. Peskin, D. V. Schroeder, *An Introduction to Quantum Field Theory*, HarperCollins Publishers, USA, 1995
- [10] ATLAS Collaboration, *ATLAS Detector and Physics Performance Technical Design Report*, CERN, 1999, available from: <http://atlas.web.cern.ch/Atlas/GROUPS/PHYSICS/TDR/access.html>
- [11] ATLAS Computing Group, *ATLAS Computing Technical Design Report*, CERN, 2005, available from: <http://atlas-proj-computing-tdr.web.cern.ch/atlas-proj-computing-tdr/PDF/Computing-TDR-final-July04.pdf>

- [12] ATLAS HLT/DAQ/DCS Group, *ATLAS High-Level Trigger, Data Acquisition and Controls Technical Design Report*, CERN, 2003, available from:  
<http://cdsweb.cern.ch/record/616089/files/cer-002375189.pdf>
- [13] The ATLAS Pixel Group, *Pixel Offline Analysis for EndcapA Cosmic Data*, CERN, 2007, available from:  
<http://cdsweb.cern.ch/record/1074907/files/indet-pub-2008-003.pdf>
- [14] Wikipedia - Feynman Diagram,  
[http://en.wikipedia.org/wiki/Feynman\\_diagram](http://en.wikipedia.org/wiki/Feynman_diagram)
- [15] Wikipedia - Nuclear Force,  
[http://en.wikipedia.org/wiki/Nuclear\\_force](http://en.wikipedia.org/wiki/Nuclear_force)
- [16] Wikipedia - Møller Scattering,  
[http://en.wikipedia.org/wiki/Møller\\_scattering](http://en.wikipedia.org/wiki/Møller_scattering)
- [17] Wikipedia - Compton Scattering,  
[http://en.wikipedia.org/wiki/Compton\\_scattering](http://en.wikipedia.org/wiki/Compton_scattering)
- [18] I. C. Brock, *Physics of and with Leptons WS 05/06 - Feynman Graphs*,  
[http://pi.physik.uni-bonn.de/~brock/feynman/vtp\\_ws0506/](http://pi.physik.uni-bonn.de/~brock/feynman/vtp_ws0506/)
- [19] M. Scherzer, *Hardware Blog*,  
<http://octopart.com/blog/get?y=2007&m=6&d=6>
- [20] The CMS and TOTEM diffractive and forward physics working group, *Prospects for Diffractive and Forward Physics at the LHC*, CERN, 2006, available from: <http://cmsdoc.cern.ch/cms/PRS/sm/diffractive-lhcc2.pdf>
- [21] NYU participation in ATLAS,  
<http://www.physics.nyu.edu/experimentalparticle/atlas.html>
- [22] ATLAS experiment public pages, <http://atlas.ch>
- [23] LHC machine outreach,  
<http://lhc-machine-outreach.web.cern.ch/lhc-machine-outreach>
- [24] CERN FAQ - LHC the guide,  
<http://cdsweb.cern.ch/record/1092437/files/CERN-Brochure-2008-001-Eng.pdf>
- [25] High energy physics in Europe, <http://highenergyparticles.net>
- [26] Wikipedia - Large Hadron Collider,  
[http://commons.wikimedia.org/wiki/Large\\_Hadron\\_Collider](http://commons.wikimedia.org/wiki/Large_Hadron_Collider)

- [27] ATLAS Twiki pages - InDet Tracking Performance Plots from the CSC Book,  
[https://twiki.cern.ch/twiki/bin/view/Atlas/  
InDetTrackingPerformanceCSCFigures](https://twiki.cern.ch/twiki/bin/view/Atlas/InDetTrackingPerformanceCSCFigures)
- [28] ATLAS Twiki pages - Running the Full Chain,  
<https://twiki.cern.ch/twiki/bin/view/Atlas/WorkBookFullChain>
- [29] ATLAS Twiki pages - Pixel Cosmic Test,  
<https://twiki.cern.ch/twiki/bin/view/Atlas/PixelCosmic>
- [30] ATLAS Twiki pages - How to run simulation of pixel endcap A cosmic,  
[https://twiki.cern.ch/twiki/bin/view/Atlas/  
HowToRunPixelEndCapCCosmicSimulation](https://twiki.cern.ch/twiki/bin/view/Atlas/HowToRunPixelEndCapCCosmicSimulation)
- [31] ATLAS Twiki pages - Cosmic simulation package documentation,  
<https://twiki.cern.ch/twiki/bin/view/Atlas/CosmicSimulation>
- [32] ATLAS Twiki pages - PixelGeoModel package documentation,  
<https://twiki.cern.ch/twiki/bin/view/Atlas/PixelGeoModel>
- [33] Geant4 ATLAS applications,  
[http://atlas-computing.web.cern.ch/atlas-computing/packages/  
simulation/geant4/G4AtlasApps/doc/](http://atlas-computing.web.cern.ch/atlas-computing/packages/simulation/geant4/G4AtlasApps/doc/)
- [34] ATLAS Twiki pages - InDetCosmicSimAlgs simulation package documenta-  
tion,  
<https://twiki.cern.ch/twiki/bin/view/Atlas/InDetCosmicSimAlgs>
- [35] ATLAS Collaboration, *Atlantis event display*,  
<http://www.hep.ucl.ac.uk/atlas/atlantis/>
- [36] HyperPhysics - Cosmic Rays,  
<http://hyperphysics.phy-astr.gsu.edu/Hbase/astro/cosmic.html#c2>
- [37] Ultra High Energy Cosmic Rays (UHECR),  
<http://www.physics.adelaide.edu.au/astrophysics/hires/uhecr.html>

